

# **First-principles calculations of Urea, MNA and TaAs**

A Project Report submitted to Department of Physics,  
St. Joseph's College (Autonomous), Tiruchirappalli,  
in partial fulfilment of the requirements for the award of the degree of

## **MASTER OF SCIENCE IN PHYSICS**

by

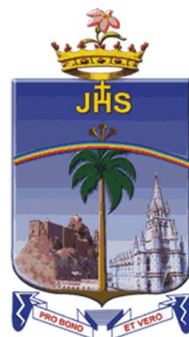
**J. JOHN PAUL**

(22PPH101)

Under the guidance of

**Dr. R. JERALD VIJAY**

Assistant Professor, Department of physics  
St. Joseph's College (Autonomous)



**DEPARTMENT OF PHYSICS**  
**St. JOSEPH'S COLLEGE (AUTONOMOUS)**

**(Affiliated to Bharathidasan University, Tiruchirappalli)**

Accredited at A<sup>++</sup> Grade (Cycle IV) by NAAC

Special Heritage Status awarded by UGC

**TIRUCHIRAPPALLI-620002**

**MARCH 2024**

**Dr. R. JERALD VIJAY**

Assistant Professor

Department of Physics

St. Joseph's College (Autonomous)

Tiruchirappalli – 620002

Date: 22-3-24

## CERTIFICATE

This is to certify that the project entitled "*First-principles calculations of Urea, MNA and TaAs*" submitted to the Department of Physics, St. Joseph's College (Autonomous), Tiruchirappalli – 620 002, in partial fulfilment for the award of the degree of Master of Science in Physics by **J. John Paul** (22PPH101), is a record of original project work carried out under my guidance and supervision.



**Dr. I. Johnson**

Head of the Department

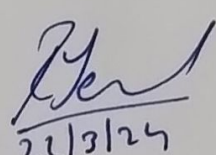
**Dr. I. JOHNSON, M.Sc., M.Phil., Ph.D.**

Head

Research Advisor & Principal Investigator

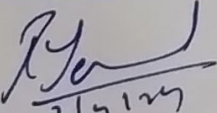
Associate Professor, Dept. of Physics

Submitted for the Viva-Voce Examination held on 24-3-24.  
Tiruchirappalli-620 002.

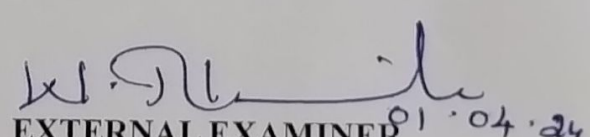


**Dr. R. Jerald Vijay**

Staff In-charge

  
**INTERNAL EXAMINER**

(Signed after the viva-voce)

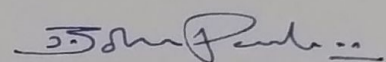
  
**EXTERNAL EXAMINER**

01.04.24

## DECLARATION

I hereby declare that the project entitled "*First-principles calculations of Urea, MNA and TaAs*" submitted to St. Joseph's College (Autonomous), Tiruchirappalli, in partial fulfilment of the requirement of the degree, is a record of original project work done by me during the period of study, under the Guidance of **Dr. R. Jerald Vijay**, Assistant Professor, Department of Physics, St. Joseph's College (Autonomous), Tiruchirappalli.

I further declare that no part of this dissertation has been submitted elsewhere for the award of any other degree.



J. John Paul

## **ACKNOWLEDGEMENT**

First and foremost, I thank God Almighty for giving me the grace to complete my course and project work successfully.

I express my gratitude to Rev. Dr. M. Arockiasamy Xavier S.J., Principal, St. Joseph's College (Autonomous), Tiruchirappalli-2, for giving me the opportunity to do study in this prestigious institution.

I show my gratitude to Dr. I. Johnson, the Head, Department of Physics, St. Joseph's College (Autonomous), Tiruchirappalli-2, for ensuring the smooth and unhindered progress of my work and providing me the opportunity to this work.

With immense pleasure, I express my deep appreciation and gratitude, to Dr. R. Jerald Vijay, Assistant Professor, Department of Physics, St. Joseph's College (Autonomous), Tiruchirappalli-2, for his constant support, guidance, and encouragement throughout this project. I express my gratitude to him for the insightful conversations we shared, which aided me in steering my work and enhancing my understanding across multiple domains within physics.

I extend my special thanks to J. Jude Felix, D. M. Satheesh, S. Ganapathy and M. J. Barath for encouraging and providing moral and technical support during work.

Finally, I wish to express my deepest gratitude to my family, my teaching and non-teaching staff members, and colleagues for their encouragement and support.

## ABSTRACT

The quest for nonlinear optical materials has increased in recent years because of their demand in various applications like high performance optoelectronic devices, quantum technologies, signal processing, and biomedical imaging. Therefore, researchers are in search of new nonlinear optical materials with unique and desired properties. This work employs Density Functional Theory (DFT) using Quantum Espresso to investigate the structural, electronic, and optical properties of urea, Methyl-4-nitroaniline (MNA), and Tantalum Arsenide (TaAs). The results reveal the band gap values for urea (~5.4 eV) and MNA (~2.2 eV), elucidating the dominant electron contributions from specific orbitals. Additionally, TaAs is identified as a Wely semimetal from its band structure, exhibiting notable bonding involving the d orbitals of Ta and As. The absorption spectra of MNA and TaAs unveils distinct electronic transitions. These findings contribute to the understanding of nonlinear optical materials and using the results obtained from this work further calculations can be carried out to calculate the applied properties.

*Keywords:* Density functional theory, electronic properties, absorption spectra, NLO martials

# Table of Contents

<b>Chapter 1: Introduction</b>	<b>1</b>
1.1. Introduction to First-principles calculation.....	1
1.2. Importance of Material Properties prediction .....	1
1.3. Objective of the work.....	2
1.4. Materials chosen.....	2
1.5. Note on organic and inorganic NLO crystals.....	3
1.6. Open-source software for First-principles calculation.....	4
1.7. Overview .....	4
<b>Chapter 2: Theoretical background of First-principles calculations</b>	<b>6</b>
2.1. First-principles method .....	6
2.2. The many-body problem.....	6
2.3. Born – Oppenheimer (BO) approximation .....	7
2.4. Mean field approach (MFT) .....	8
2.4.1. Hartree method .....	9
2.5. Self-Consistent field (SCF) method .....	9
2.5.1. Hartree-Fock (HF) approximation .....	10
2.6. Density functional theory (DFT) .....	11
2.6.1. Electron density .....	12
2.6.2. Density functional not density function .....	13
2.6.3. Hohenberg and Kohn (HK) theorems .....	13
2.6.4. The Kohn-Sham ansatz .....	14
2.6.5. Energy terms.....	16
2.6.5.1. Kinetic energy.....	16
2.6.5.2. External energy .....	16
2.6.5.3. Hartree energy .....	16
2.6.5.4. Exchange-correlation (XC) energy .....	17
2.6.6. Kohn-Sham equations .....	17
2.6.6.1. KS non-interacting electrons .....	19
2.6.6.2. KS orbital and KS eigenvalues .....	19

2.7.	Exchange correlation functional .....	20
2.7.1.	Local density approximation (LDA) .....	20
2.7.2.	Generalized gradient approximation (GGA) .....	21
2.7.3.	Perdew, Burke and Ernzerhof (PEB) approximation .....	21
2.7.4.	Other XC functionals.....	22
<b>Chapter 3: Tools and techniques</b>		<b>24</b>
3.1.	The plane wave basis set.....	24
3.1.1.	Periodic systems and Bloch's theorem .....	24
3.1.2.	The plane wave expansion .....	27
3.1.3.	Truncating the PW expansion .....	28
3.1.4.	K-points and sampling the first BZ .....	29
3.2.	Pseudopotentials (PPs).....	29
3.3.	Units used in DFT .....	31
3.4.	Quantum ESPRESSO (QE) code.....	32
3.4.1.	The QE SCF Iterative solution.....	33
3.4.2.	Parameters for QE input file for SCF calculation .....	34
3.5.	The control block of QE.....	37
3.6.	The QE input file.....	38
3.7.	Running the QE package.....	39
3.8.	The QE output file.....	39
3.9.	Structural optimization using QE and VESTA .....	42
3.10.	Calculation for DOS, PDOS and Band structure .....	43
3.10.1.	Selecting the high symmetry K-points.....	44
3.11.	Calculation of Absorption spectra.....	46
3.12.	System Parameters .....	47
3.13.	Other tools used .....	48
3.13.1.	VESTA .....	48
3.13.2.	XCrySDen.....	48
3.13.3.	Python .....	49
3.13.4.	BURAI.....	49

3.13.5. Origin.....	50
3.13.6. Fortran.....	50
3.13.4. FFT and LAPACK .....	50
<b>Chapter 4: First-principles calculations of UREA and 2-methyl-4-nitroaniline</b>	<b>51</b>
4.1. Organic crystals.....	51
4.2. Urea.....	52
4.2.1. Crystal structure of urea.....	52
4.2.2. Electronic properties of Urea .....	54
4.3. 2-methyl-4-nitroaniline (MNA) .....	56
4.3.1. Crystal structure .....	57
4.3.2. Electronic property of MNA .....	59
4.3.3. Absorption spectra of MNA.....	61
<b>Chapter 5: First-principles calculations of Tantalum Arsenide</b>	<b>63</b>
5.1. Inorganic crystals .....	63
5.2. Tantalum Arsenide (TaAs).....	64
5.3. Structural parameters .....	64
5.4. Mechanical properties .....	66
5.5. Electronic Properties .....	66
5.6. Magnetic properties.....	69
5.7. Thermodynamic property.....	70
5.8. Absorption spectra .....	70
<b>Chapter 6: Conclusion and further work</b>	<b>71</b>
6.1. Conclusion .....	71
6.2. Further work.....	72
<b>Reference</b>	<b>73</b>

# CHAPTER 1

## Introduction

### 1.1. Introduction to First-principles calculation

In the field of materials science, the ability to predict and understand the properties of materials at the atomic and electronic levels is paramount for the design and development of new materials with tailored functionalities. Traditionally, experimental techniques have played a central role in characterizing materials, but they are often limited in their ability to provide detailed insights into the underlying atomic and electronic structures. In recent decades, computational methods based on first principles-principles have emerged as powerful tools for studying the properties of materials from fundamental physical principles. These methods, which rely on the laws of quantum mechanics and do not incorporate any empirical parameters or experimental data it offers a comprehensive and accurate approach to modelling the behaviour of materials at the atomic scale.

The central part of first-principles calculations lies the concept of Density Functional Theory (DFT), a quantum mechanical theory that provides a framework for describing the electronic structure of materials. In DFT, the electronic density serves as the central quantity, and the total energy of the system is expressed as a functional of this density. By solving the Kohn-Sham equations, which are derived from the variational principle, DFT allows for the determination of the ground-state electronic structure of a material, including the distribution of electrons and their energies.

One of the key advantages of first-principles calculations is their ability to predict a wide range of material properties without the need for experimental input. From structural properties such as lattice parameters and bond lengths to electronic properties such as band structures and density of states, first principles methods provide valuable insights into the behaviour of materials under different conditions.

### 1.2. Importance of Material Properties prediction

The prediction of material properties holds immense importance in various fields of science and engineering. Here are some key reasons why material properties prediction is crucial:

- **Materials Design and Development:** Predicting material properties allows researchers to design and develop new materials with desired characteristics tailored for specific applications. By understanding how atomic and electronic structures influence material behaviour, scientists can engineer materials with enhanced properties such as strength, conductivity, and durability.
- **Optimization of Existing Materials:** Material properties prediction enables the optimization of existing materials to improve their performance and functionality.
- **Efficient Resource Utilization:** Predictive modelling of material properties reduces the need for costly and time-consuming experimental trials by guiding researchers towards promising candidates for further investigation. This helps in conserving resources and accelerating the materials discovery process.
- **Technological Innovation:** Predictive modelling provides insights into the potential performance of materials in diverse environments and applications, fostering the creation of new technologies and products.
- **Understanding Fundamental Science:** Material properties prediction contributes to a deeper understanding of fundamental scientific principles governing the behaviour of matter at the atomic and electronic levels. By elucidating the underlying mechanisms and interactions that dictate material properties, researchers can advance our knowledge of condensed matter physics, chemistry, and materials science.
- **Addressing Societal Challenges:** By developing materials with tailored properties, researchers can create solutions for clean energy technologies, pollution mitigation, and biomedical applications.

### **1.3. Objective of the work**

- To Understand the Theoretical framework of first principles calculations using density functional (DFT) theory.
- To develop optimized structure of materials.
- To calculate the various properties of materials using First-principles calculations.

### **1.4. Materials chosen**

Initially, a diverse range of materials was considered for study, but later, Urea, MNA, and TaAs were selected. Literature review revealed that performing first-principles calculations on organic crystals is challenging and, presenting a significant opportunity for exploration, and understanding [1] [2]. TaAs was chosen due to its versatile properties and it

is a recently developed material [3] [4]. It holds promise for various applications such as being a topological insulator, Weyl semimetal, and nonlinear optical properties including second harmonic generation (SHG) and terahertz (THz) generation. Consequently, investigating TaAs offers extensive potential across multiple fields. All the three materials have potential application in non-linear optics.

## 1.5. Note on organic and inorganic NLO crystals

Organic NLO crystals are composed of carbon-based molecules arranged in a periodic lattice structure. These crystals exhibit strong nonlinear optical properties arising from the delocalized pi-electron system within the molecules. Due to the presence of conjugated double bonds and charge transfer interactions, organic NLO crystals often display large hyperpolarizabilities, which enable efficient frequency conversion processes such as second harmonic generation (SHG) and optical parametric amplification (OPA). Organic NLO crystals offer advantages such as tuneable optical properties, flexibility in molecular design, and relatively easy synthesis methods. They find applications in nonlinear optics, photonics, telecommunications, and biological imaging. Despite their many advantages, organic NLO materials also present challenges, including limited thermal and photochemical stability, as well as relatively low nonlinear optical coefficients compared to some inorganic materials. Ongoing research efforts focus on addressing these challenges through the development of new molecular designs, advanced fabrication techniques, and hybrid organic-inorganic systems.

Inorganic NLO crystals are composed of metal, metal oxide, or semiconductor atoms arranged in a crystalline lattice structure. These crystals possess strong nonlinear optical properties due to symmetry-breaking effects and electronic transitions within the crystal lattice. Inorganic NLO crystals often exhibit high laser damage thresholds, thermal stability, and optical transparency over a broad spectral range. They are utilized in various applications such as frequency doubling, optical switching, electro-optic modulation, and photonic integrated circuits. Inorganic NLO crystals offer advantages such as high efficiency, robustness, and suitability for high-power laser applications. Despite their many advantages, inorganic NLO materials also present challenges, including limitations in phase-matching conditions, crystal growth techniques, and processing complexities. Ongoing research efforts focus on overcoming these challenges through the development of novel crystal growth methods, engineered microstructures, and hybrid material systems.

Nonlinear optical (NLO) materials play a crucial role in harnessing and manipulating THz radiation for these applications. One of the key applications of THz radiation is in THz spectroscopy, which provides valuable information about the molecular structure, dynamics, and interactions of materials. Nonlinear optical materials can be used to generate and detect THz radiation through nonlinear optical processes such as difference frequency generation (DFG) and optical rectification.

## 1.6. Open-source software for First-principles calculation

Open-source Density Functional Theory (DFT) software represents a valuable resource for researchers in the fields of computational chemistry, condensed matter physics, and materials science. These software packages provide powerful tools for performing first-principles calculations to predict the electronic structure and properties of materials from fundamental principles, without the need for proprietary software or expensive licenses. One of the key advantages of open-source DFT software is its accessibility and affordability, making advanced computational techniques available to a wide range of users, including academic researchers, students, and industry professionals. Additionally, open-source software encourages collaboration, transparency, and community-driven development, leading to the continuous improvement and refinement of computational methods and algorithms. In this work several open-source software and codes are used to calculate the properties of materials [5].

## 1.7. Overview

This project presents a comprehensive investigation into the theoretical foundations of First-principles calculations using Density functional theory (DFT), tools and techniques to perform first-principles calculations using Density Functional Theory (DFT). The study focuses on applying these methods to elucidate the electronic and structural properties of two organic crystals, Methyl-4-nitroaniline (MNA) and Urea, as well as the recently developed inorganic material Tantalum Arsenide (TaAs).

The second chapter delves into the theoretical aspects of first-principles calculations, with a particular emphasis on Density Functional Theory (DFT). The chapter begins by introducing the in-depth discussion of the DFT formalism. Key concepts such as the Kohn-Sham equations and exchange-correlation functionals.

The third chapter gives a comprehensive overview of the tools and techniques utilized in first-principles calculations is presented. The chapter covers a range of topics, including

software packages for performing DFT calculations, preprocessing of input files, selection of appropriate computational parameters, and post-processing of simulation results. Additionally, advanced techniques such as plane-wave basis sets, pseudopotential approximation methods, and convergence testing are discussed in detail to provide insights into the computational strategies employed in the study.

The fourth chapter focuses on the application of first-principles calculations to investigate the electronic and structural properties of MNA and Urea, two organic crystals of interest. The chapter begins with an overview of the materials. The results obtained from the calculations are then presented and analysed, providing insights into the electronic band structures, density of states, and optical properties of MNA and Urea.

The fifth chapter focus to Tantalum Arsenide (TaAs), a recently developed inorganic material with promising properties for various applications. The chapter begins with an overview of the materials. The results obtained from the calculations are then presented and analysed, providing insights into electronic band structures, topological properties, and nonlinear optical behaviour of TaAs.

## CHAPTER 2

### Theoretical background of First-principles calculations

#### 2.1. First-principles method (ab-initio method)

First-principles calculation method is based on quantum mechanics, which does not use any fitting parameters from experimental data and is only based on the fundamental information like atomic number, charge, mass, coulomb force, etc. of the constituent atoms. First-principles calculation method is purely based on the fundamental Hamiltonian of the system. The First-principles calculation yields a non-empirical result, i.e., this calculation derives physical properties without introducing adjustment parameters.

There are various methods to perform ab-initio calculations like semi-empirical methods, Hartree-Fock methods, tight binding method, density functional theory, quantum Monte Carlo methods and couple cluster methods. In the following, the theory explaining first principles calculations using Density functional theory (DFT) is being discussed.

#### 2.2. The many-body problem

In theoretical condensed matter physics one can fundamentally estimate physical properties of solids by solving the corelated many-body Schrödinger equation.

$$\hat{H}\psi = E\psi \quad (2.1)$$

In this particular case the Hamiltonian operator  $\hat{H}$  of a solid is made up of interacting nuclei and electrons.

$$\hat{H} = -\frac{1}{2} \left[ \left( \sum_I \frac{\hbar^2}{M_I} \nabla_I^2 + \sum_i \frac{\hbar^2}{M_i} \nabla_i^2 \right) + \left( \sum_{i,\alpha} \frac{Z_I e^2}{|\vec{r}_i - \vec{R}_I|} - \sum_{i \neq j} \frac{e^2}{|\vec{r}_i - \vec{r}_j|} - \sum_{I \neq J} \frac{Z_I Z_J e^2}{|\vec{R}_I - \vec{R}_J|} \right) \right] \quad (2.2)$$

Where,  $\vec{R}$  represents the coordinates of nuclei,  $\vec{r}$  represents the coordinates of electrons. The first two terms are the kinetic energy operators for nuclei and electron the next three terms represents the interactions between nuclei-electron, electron-electron, nuclei-nuclei [6].

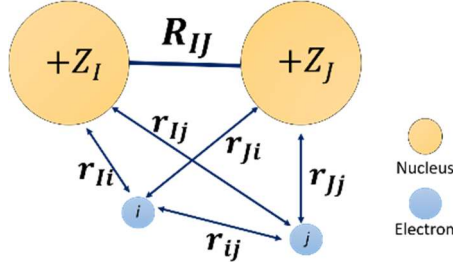


Fig 2.1: The interactions of electrons and nuclei in an atom

### 2.3. Born – Oppenheimer (BO) Approximation

As nuclei possess significantly greater mass than electrons, their positions within a system are generally approximated as fixed, while the positions of electrons are dynamic, due to their relatively lighter mass compared to nuclei. When same momentum is applied to the nuclei and electron the relative motion of electrons w.r.t that of nuclei is faster. The electrons adiabatically do not experience any transitions between stationary states. By this the many body Schrödinger equation can be decoupled to the nuclear degrees of freedom and electronic degree of freedom. This is called as Born-Oppenheimer (BO) or adiabatic approximation. Here adiabatic means there is no coupling between different electronic surface.

The BO approximation involves representing the wavefunction of a molecule as the product of an electronic wavefunction and a nuclear wavefunction. This approach facilitates the division of the Hamiltonian operator into electronic and nuclear components, disregarding cross-terms between electrons and nuclei. As a result, the two smaller and independent systems can be solved more effectively. That is in equation (2.2) the last term becomes constant and can be merged into the third term to be the fixed potential external to electrons,  $V^{ext}(\vec{r}, \vec{R})$ .

Therefore, the equations (2.1) and (2.2) explicitly becomes

$$\hat{H}_e \psi_e(\vec{r}, \vec{R}) = E_e \psi_e(\vec{r}, \vec{R}) \quad (2.3)$$

Where  $\hat{H}_e$  represents the Hamiltonian of interacting electrons subject to external potential created by the nuclei which can be called as clamped Schrödinger equation.

$$\hat{H}_e = - \sum_I \frac{\hbar^2}{2M_I} \nabla_I^2 + \frac{1}{2} \sum_{i \neq j} \frac{e^2}{|\vec{r}_i - \vec{r}_j|} + V^{ext}(\vec{r}, \vec{R}) \quad (2.4)$$

After BP approximation the number of degrees of freedom of  $\hat{H}$  is significantly reduced. The (2.4) is not a direct equation to solve further approximation methods must be applied on the equation to solve realistic systems.

Since in this approximation the nuclei is constant w.r.t electronic motions, this constant when added to the Hamiltonian, the Hamiltonian shifts by the value of the constant.

$$(\hat{H} + C)\psi = (E + C)\psi \quad (2.5)$$

Thus (2.4) can be written as

$$\hat{H}_e = \hat{T}_e(\vec{r}) + V_{ee}(\vec{r}) + V^{ext}(\vec{r}, \vec{R}) + V_{NN}(\vec{R}) \quad (2.6)$$

Where  $\hat{T}_e(\vec{r})$  is the kinetic energies of the electronic interaction,  $V_{ee}(\vec{r})$  is the potential energy of the electronic interaction,  $V^{ext}(\vec{r}, \vec{R})$  the fixed potential external to electrons due to nuclei and  $V_{NN}(\vec{R})$  is the nuclear repulsion energy which is a constant.

Consider (2.2) the original Hamiltonian. An exact solution can be obtained by using an infinite expansion of the form

$$\psi_e(\vec{r}, \vec{R}) = \sum_k \psi_k(\vec{r}, \vec{R}) \chi_k(\vec{R}) \quad (2.7)$$

To the extent of BO approximation vary accurate solutions can be obtained using only one or few terms. Here  $\chi_k(\vec{R})$  is the nuclear wavefunction.

In general, the electrons are treated as quantum particles in the field of fixed or slowly varying nuclei. Now inserting (2.7) in (2.2) we have the following

$$[\hat{T}_N(\vec{R}) + T''_{kk}(\vec{R}) + E_e(\vec{R})]\chi_k(\vec{R}) = E\chi_k(\vec{R}) \quad (2.8)$$

Were  $\hat{T}_N(\vec{R})$  is the electronic kinetic energy,  $T''_{kk}(\vec{R})$  is the nonadiabatic coupling term used for correction and  $E_e(\vec{R})$  is the expatiation value of electronic energy which is essentially the potential felt by the nuclei. Now solving (2.8) will yield the electronic energy.

Computationally this becomes expensive to solve so we go for further approximations [6].

## 2.4. Mean field approach (MFT)

The main idea of MFT is to replace all the interactions to one body with an average or effective interaction. It is assumed that every single particle in the system only experiences

the average behaviour of its neighborhood MFT the Hamiltonian can be expanded in terms of the magnitude of the fluctuations around the mean of the field which can be considered as a zeroth order expansion of the Hamiltonian. This all the interactions are replaced by a mean field. Mostly it is done by replacing the interaction terms with quadratic terms for obtaining exactly solvable Hamiltonian [7].

#### **2.4.1. Hartree method**

In this context consider each electron moving in an effective potential representing the attraction of the nuclei and the average field of repulsive interactions of the other electrons this type of model is called as the independent particle model or the Hartree model. In this the average repulsion is the electrostatic repulsion of the average charge density of all other electrons.

In Hartree method it is assumed the nucleus together with the electrons form a spherically symmetric field. Then the charge distribution of each electron would be the solution of the Schrödinger equation for an electron potential derived from the field. Consider each particle is in different orbital so that the wavefunction in a product form

$$\psi(x_1, x_2, x_3, \dots, x_p) = \psi_\alpha(x_1)\psi_\beta(x_2)\psi_\gamma(x_3)\dots\psi_\pi(x_p) \quad (2.9)$$

Where  $x_1, x_2, x_3, \dots, x_p$  are the coordinates of the electrons and  $\alpha, \beta, \gamma, \dots, \pi$  are the states of the electrons. (2.9) is called as the Hartree product which gives the wavefunction of the many-particle system as a combination of wavefunction of individual particles. It is inherently a mean field and it assumes that the electrons are independent particles. Although it is simplifying the calculation, Hartree produce yields a wave function which is symmetric it is not applicable for fermions as they have antisymmetric nature [8].

#### **2.5. Self-Consistent field (SCF) Method**

As the real wavefunction is complex to solve, it is approximated by a simpler wavefunction this enables the electronic Schrödinger equation (equation of the form (2.9)) to be solved numerically. The self-consistent field method is an iterative method that involves selecting an approximate Hamiltonian, solving the Schrödinger equation to obtain more accurate set of orbitals, then solving the Schrödinger equation until the results converge.

Here the idea is not to describe the interaction of one of the particles with all of the other particle individually rather only the interaction with the distribution of the particles. The

Hartree method is a SCF method in which it depends on the orbitals that are the solution of all other Hartree equations i.e., there are n simultaneous intero-differential equations for n orbitals and the solution is achieved iteratively.

The iterations are carried in the following way, initial guess of orbitals, constructing the operator, solution of single particle pseudo-Schrödinger equation, obtaining new set of orbitals and constructing the operators, this iteration is followed till the convergence is achieved [8].

### 2.5.1. Hartree – Fock (HF) approximation

As Hartree method lack in the anti-symmetric property for fermions a set of identical indistinguishable fermions has a wavefunction that is antisymmetric by exchange can be given as

$$\psi(\vec{x}_1, \vec{x}_2, \dots, \vec{x}_j, \dots, \vec{x}_k, \dots, \vec{x}_n) = -\psi(\vec{x}_1, \vec{x}_2, \dots, \vec{x}_k, \dots, \vec{x}_j, \dots, \vec{x}_n) \quad (2.10)$$

The N-body wavefunction of the system can be approximated by a single *Slater determinant* (expression that describes the wavefunction of a multi-fermionic system satisfying anti-symmetry and Pauli principle) of which the elements are one-electron wavefunctions  $\psi_1, \psi_2, \dots, \psi_N$  for N-electron can be defined and a suitable ansatz can be applied to invoke the variational method and the set of N-coupled equations for N spin orbitals can be determined. The solution of these equations yields the Hartree-Fock wavefunction and energy of the system. The high order fluctuation can be neglected which allows the interaction terms to be replaced with quadratic terms obtaining exactly solvable Hamiltonians. The Slater determinant can be written as

$$\psi_{HF}(\vec{x}_1, \vec{x}_2, \dots, \vec{x}_N) = \begin{vmatrix} \psi_1(1) & \psi_2(2) & \cdots & \psi_N(1) \\ \psi_1(2) & \psi_2(2) & \cdots & \psi_N(2) \\ \vdots & \vdots & \ddots & \vdots \\ \psi_1(N) & \psi_2(N) & \cdots & \psi_N(N) \end{vmatrix} \quad (2.11)$$

Where the variable  $x$  contains both spital ( $\vec{r}$ ) and the spin coordinates ( $s$ ),  $\psi_i(j)$  defines the one-electron wavefunction of the  $i^{th}$  electron at the position of the  $j^{th}$  electron. The antisymmetric is achieve by interchange of the coordinates of two electrons.

By using the *variational method* to minimize the expatiation value of the Hamiltonian (2.4) under the orthonormality constraint of single-particle wavefunction the HF equation is obtained as

$$\left[ -\frac{\hbar^2}{2M_I} \nabla_I^2 + V^{ext}(\vec{r}, \vec{R}) + \sum_j \int d\vec{r}' \psi_j^*(\vec{r}') \psi_j(\vec{r}') \frac{e^2}{|\vec{r}_I - \vec{r}_j|} \right] \psi_i(\vec{r}') \\ + \sum_j \int d\vec{r}' \psi_j^*(\vec{r}') \psi_i(\vec{r}') \frac{e^2}{|\vec{r}_I - \vec{r}_j|} \psi_j(\vec{r}) \delta_{s_i s_j} = \epsilon_i \psi_i(\vec{r}') \quad (2.12)$$

The HF approximation explicitly considers the prescription of electron exchange energy as denoted by the last term. The solution can be solved by the self-consistent field approach because the HF theory is based on one electron subject to the average potential created by the nucleus and other electrons.

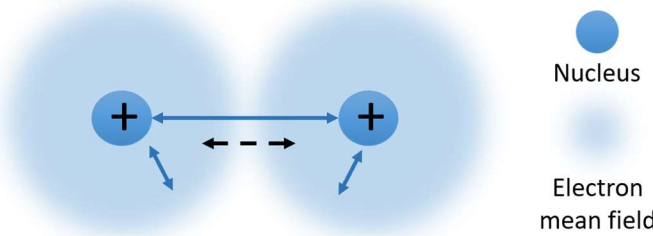


Fig 2.2: Schematic of the Hartree–Fock model with the exchange energy counted by the Slater determinant expression for the wave function

HF theory ignores the inherent electron corelation i.e. the dynamical corelation where the electrons get too close to each other and static corelation where the determinant variational class is not good. Apart from this there is spin contamination in mixing different spin states. The density functional theory is an approach to incorporate the exchange and corelation effects which is discussed in the upcoming sections [9] [10].

## 2.6. Density functional theory (DFT)

DFT was developed based on original idea introduced by Thomas and Fermi in 1927 and the theoretical framework was developed by Walter Kohn and Pierre Hohenberg using the Hohenberg-Kohn theorems (HK) [10].

Unlike the wave function based on HF approximation the electron density is considered as the basic variable to uniquely determine the many-body system in the ground state. The DFT relies on the theorems proposed by Hohenberg and Kohn. In the quantum mechanical view, the N-body problem is now an electron-density-dependent problem [8].

## 2.6.1. Electron density

Electron density is the measure of the probability of an electron being present at an element of space surrounding an atom or molecule. By nature, it is a scalar quantity. As a consequence of uncertainty principle, the exact location of electron is not possible to predict only the probability of existing in a given position is possible. Therefore atoms and molecules in the system appears as if they are smeared out in space.

Specifically, the electron density  $n(\vec{r})$  in an N-electron system is the number of electrons per unit volume at a given point  $\vec{r}$ . For one-electron system the electron density at any point is proportional to the square magnitude of the wavefunction. The core-electron densities are localized very near the nucleus and the valence-electron densities are diffused.

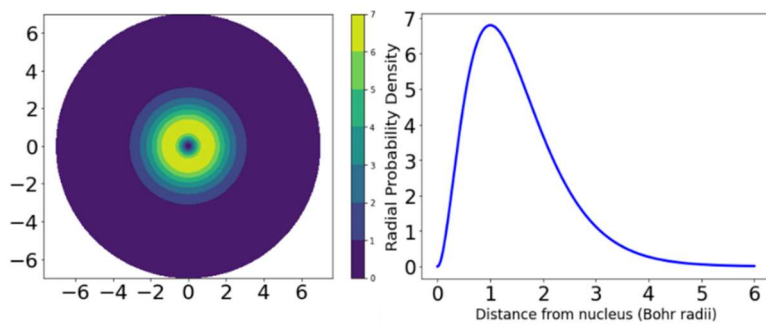


Fig 2.3: 2D Representation of the electronic density of hydrogen atom (Made using Python)

Electron density can be visually represented by an isosurface, whereas visualising the wavefunction formed by the Hamiltonian in the previous theories is not possible. Therefore, the electron density has an observable nature in a classical and quantum mechanical view.

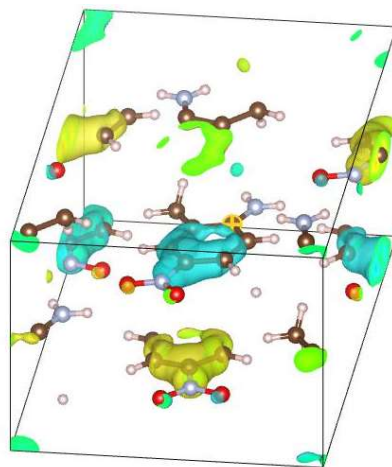


Fig 2.4: The approximate electronic charge density of MNA molecule in bulk form (Calculations performed using QE and visualized using VESTA)

Consider the electrons in the system are noninteracting, in a noninteracting reference frame with decoupled coordinates, the electron density is written as a sum over a set of squares of occupied noninteracting orbitals  $\varphi_i$

$$n(\vec{r}) = \sum_i |\varphi_i(\vec{r})|^2 = 2 \sum_i^{ocp} |\varphi_i(\vec{r})|^2 \quad (2.13)$$

Here the usual wavefunction  $\psi_i$  is replaced by orbitals  $\varphi_i$ , tis orbitals are called as the KS orbitals. From the above equation the amplitudes (positive or negative) of each orbital is converted to a positive density of electrons. If all the electron densities over the whole space is added up it will result in the total number of electrons  $n$

$$\int n(\vec{r}) dr = n \quad (2.14)$$

If ones know the atomic density the electron density of a system can be roughly estimated. the electron density in a system not only represents wave function, orbital, and the total number of electrons, but is also directly related to potentials, energies, and thus all properties of the system [9].

### 2.6.2. Density functional not Density function

A functional is a function of a function. In DFT the functional is the electron density which is a function of space and time. The function takes a function as its input and outputs a single number for example

$$F[f(x)] = \int_{-1}^1 f(x) dx \text{ where } f(x) = x^2 + 1 \text{ we get ; } F[f(x)] = \frac{8}{2}$$

Therefore, in DFT we have *electron density[space, time]* generally the time is static in DFT and position is used to find the density.

### 2.6.3. Hohenberg and Kohn (HK) theorems.

**Theorem 1:** For any system of interacting particles in an external potential  $V_{ext}(\vec{r})$  is determined by unique functional of the ground state of the particle density  $n_0(\vec{r})$ .

**Theorem 2:** The energy functional that gives the ground state energy of the system gives the lowest energy only when the input density is in the ground state.

$$E[n(\vec{r})] = F_{HK}[n(\vec{r})] + \int V_{ext}(\vec{r})n(\vec{r})d\vec{r} \quad (2.15)$$

The  $n_0(\vec{r})$  and  $V_{ext}(\vec{r})$  are related to each other by the following ideas.  $V_{ext}(\vec{r})$  measures the interactions between nuclei and electrons, the number of electrons that are interacting with nuclei is defined by the integral part of electron density  $(\cdot)$ . When seen from the electrons viewpoint these relations very evident and valid to replace the traditional Hamiltonian by the electron density. Thus, the ground state expectation value of any physical observable is a unique functional of the ground-state electron density  $n_0(\vec{r})$ .

The second theorems like a guessing game to identify the minimum energy of a system using variational principle. At a given  $V_{ext}(\vec{r})$  the energy is minimized by varying the electron density at one point it reaches the minimum state and the density at that point is  $n_0(\vec{r})$ . This guessing can start from any point usually for solids it is the electron density generated by overlapping atomic densities. In practically not possible to visualize the ground state density but it exists in the system. Here the term  $F_{HK}[n(\vec{r})]$  includes all the internal energies of the interacting particle system [10].

#### 2.6.4. The Kohn-Sham ansatz

Using HK theorems, the many-electron problem is changed to independent particle problem. This approximation is not reliable because the kinetic energy is poorly defined in terms of electron density. Using HK theorems Kohn-Sham (KS) constructed fictitious one-electrons to overcome the approximation problem. The KS ansatz states that the ground state of the original interacting system can be mapped into a referenced system of non-interacting electrons with equivalent ground state density. Thus, KS equation is a non-interacting Schrödinger like equation of a fictitious system (KS system) of non-interacting articles that generate the same density as any given system of interacting particles.

In KS ansatz each electron moves independently in a potential created by the nuclei and rest of the electrons. The interacting kinetic energy is replaced by non-interacting kinetic energy, the full electron-electron interaction is replaced by the Hartee potential. All the remaining difficult many-body terms are combined into an exchange-corelation function.

The universal functional in (2.15) can be written as

$$F[n(\vec{r})] = T_0[n(\vec{r})] + \frac{1}{2} \int d^3 r d^3 r' \frac{n(\vec{r})n(\vec{r}')}{|\vec{r} - \vec{r}'|} + E_{xc}[n(\vec{r})] \quad (2.16)$$

Where  $T_0[n(\vec{r})]$  is the independent-particle kinetic energy and  $E_{xc}[n(\vec{r})]$  is the exchange corelation energy functional. On putting (2.16) into (2.15) the KS functional is obtained

$$E_{ks}[n(\vec{r})] = F_{HK}[n(\vec{r})] + \int V_{ext}(\vec{r})n(\vec{r})d\vec{r} + \frac{1}{2} \int d^3r d^3r' \frac{n(\vec{r})n(\vec{r}')}{|\vec{r} - \vec{r}'|} + E_{xc}[n(\vec{r})] \quad (2.17)$$

Minimizing this energy functional with respect to  $n(\vec{r})$  under the constrain of fixed total number of electrons the effective potential of a non-interacting electron is obtained

$$V_{eff}(\vec{r}) = V_{ext}(\vec{r}) + \int \frac{n(\vec{r})}{|\vec{r} - \vec{r}'|} d\vec{r}' + \frac{\delta E_{xc}}{\delta n(\vec{r})} \quad (2.18)$$

Now the one-electron Schrödinger equation can be solved

$$\left[ -\frac{\hbar^2}{2m} \nabla^2 + V_{eff}(\vec{r}) \right] \psi_i(\vec{r}) = \varepsilon_i \psi_i(\vec{r}) \quad (2.19)$$

The ground state charge density and the kinetic energy functional of the non-interacting system are determined by the KS orbitals  $\psi_i(\vec{r})$  as

$$n(\vec{r}) = 2 \sum_{i=1}^{\frac{N}{2}} |\psi_i(\vec{r})|^2 \quad (2.20)$$

$$T_0[n(\vec{r})] = -2 \frac{\hbar^2}{2m} \sum_{i=1}^{\frac{N}{2}} \int \psi_i^*(\vec{r}) \frac{\partial^2 \psi_i(\vec{r})}{\partial \vec{r}^2} d\vec{r} \quad (2.21)$$

$N$  is the number of electrons in the non-magnetic system as  $n(\vec{r})_\uparrow = n(\vec{r})_\downarrow, \frac{N}{2}$  represents the lowest-lying orbital states that two electrons of opposite spin are accommodated. In a periodic system, the index  $i$  represents the set of valence bands and wave vector  $\vec{k}$  in the first Brillouin zone. The KS theory can be generalized to collinear magnetic system by considering that the electron density is constituted by two independent spin densities.

The KS theory heavily relies on the picture of non-interacting electron moving in the effective potential created by nuclei and other electrons. So, one can solve KS equations by using self-consistent field procedure by providing the exact form of  $E_{xc}[n(\vec{r})]$  is given. The effective potential generated from the guessed value of the initial density and the KS equation is subsequently solved to obtain the KS orbitals. The resulting orbitals are used to recalculate the density and the mixed with the old density and this iterative process is followed [10] [6].

## 2.6.5. Energy terms

### 2.6.5.1. Kinetic Energy

The kinetic energy in the non-interacting KS system can be expressed as summation form with the KS orbitals  $\varphi_i(\vec{r})$

$$E_{kin} = -\frac{1}{2} \sum_{i=1}^n \varphi_i^*(\vec{r}) \nabla^2 \varphi_i(\vec{r}) \quad (2.22)$$

In general, the second-order derivative operation on the orbital restricts the writing the conjugate of the orbital but in KS system the uses (2.13) write the orbitals so, this becomes a dependent parameter of density functional. As the KS approach calculates the kinetic energy in terms orbitals under one-electron scheme, thus the kinetic energy can be evaluated precisely. The neglected kinetic energy terms will be included in the Exchange corelation term [10].

### 2.6.5.2. External energy

The external potential  $U_{ext}(\vec{r})$  arises from the interaction between an electron and other nuclei. Then the external energy is calculated as the expatiation value of  $U_{ext}(\vec{r})$ . It is obtained by multiplying  $U_{ext}(\vec{r})$  from the left of the orbitals and integrating it all over the space

$$E_{ext}[n(\vec{r})] = \int \varphi_i^*(\vec{r}) U_{ext}(\vec{r}) \varphi_i(\vec{r}) dr = C \int n^{5/3}(\vec{r}) dr \quad (2.23)$$

Here  $E_{ext}[n(\vec{r})]$  is a functional that is it is a function of  $n(\vec{r})$ , which is a function of electronic coordinates. Therefore, external energy is formally expressed in terms f electron density as the only variable [10].

### 2.6.5.3. Hartree energy

The Hartree potential comes from the interaction between an electron at  $r$  and the mean electron density at  $r'$  in mean-field approximation

$$U_H(\vec{r}) = \int \frac{n(\vec{r}')}{|\vec{r} - \vec{r}'|} dr' \quad (2.24)$$

With reference to this potential the Hartree energy can be expressed as the expatiation value

$$E_H[n(\vec{r})] = \int U_H(\vec{r}) n(\vec{r}) dr = \frac{1}{2} \iint \frac{n(\vec{r}) n(\vec{r}')}{|\vec{r} - \vec{r}'|} dr dr' \quad (2.25)$$

The energy calculated this way is purely classical and Coulombic. Since any electron induced in all other electrons the energy is double counted and the result is non physical self-interaction. The self-interaction terms are taken into account in the exchange corelation function [10].

#### 2.6.5.4. Exchange-correlation (XC) energy

The XC energy consist of all quantum effects and are approximated in terms of electron density

$$E_{xc} = E_x + E_c \quad (2.26)$$

Here  $E_x$  is the exchange energy between electrons with same spin which is associated with Pauli exclusion principle which is equivalent to the wave function's antisymmetric nature w.r.t the exchange of any two electrons coordinates and  $E_c$  is the correlation energy between electrons with different spins.

The resulting exchange energy is the sum the four-centre integrals as a function of single-particle orbitals

$$E_x = -\frac{1}{2} \sum_{ij}^n \iint \frac{\varphi_i(\vec{r})^* \varphi_j^*(\vec{r}') \varphi_i(\vec{r}) \varphi_j(\vec{r})}{|\vec{r} - \vec{r}'|} dr dr' \quad (2.27)$$

This will lead to less overlapping of electron densities around the reference electron thus the electron-electron repulsion energy will be reduced. The net effect is attractive as indicated by the negative sign. (2.27) is always calculated approximately w.r.t the computational convergence because exactly calculating it would follow the HF method which deviates from the DFT [10].

Two electrons with different spin can occupy the same orbital, however they also repel each other because of the same negative charges this is called as the *electronic correlation*. Due to this correlation, it results in less overlapping of electron density generating a small attractive energy.

#### 2.6.6. Kohn-Sham equations

The energy expression is given as the expectation value of  $\hat{H}$  which is obtained by solving the Schrödinger equation

$$E = \int \psi^* \hat{H} \psi dr \quad (2.30)$$

Further the wave function is subjected to the orthonormal constraint

$$\int \psi_i^*(r) \psi_j(r) dr = 1 \text{ at } i = j, 0 \text{ and at } i \neq j \quad (2.31)$$

On applying the variational principle with a Lagrange multiplier  $\lambda$  with normality constraint on the energy equation, the energy equation returns to the Schrödinger wave equation (2.1)

$$0 = \delta \left( \int \psi^* \hat{H} \psi dr \right) = \delta \left[ \int \psi^* \hat{H} \psi dr - \lambda \left( \int \psi_i^* \psi_i dr - 1 \right) \right] \rightarrow \hat{H} \psi = E \psi \quad (2.32)$$

The same procedure is followed to obtain the KS equations, starting with the energy functionals of DFT. At minimum energy, the variation of the energy functional is zero w.r.t wave function or electron density

$$0 = \frac{\delta E[n(r)]}{\delta \varphi_i^*(r)} = \frac{\delta}{\delta \varphi_i^*(r)} \left[ E[n(r)] - \sum_{ij} \lambda_{ij} \left[ \int \varphi_i^*(\vec{r}) \varphi_j(\vec{r}) dr \right] \right] \quad (2.33)$$

Here the Lagrange multiplier  $\lambda_{ij}$  ensures the orthonormality constraint for orbitals. By rearranging and substituting potentials for corresponding energy functionals we have

$$0 = \frac{\delta E_{kin}^{non}}{\delta \varphi_i^*(r)} + \left[ \frac{\delta E_{ext}}{\delta n(r)} + \frac{\delta E_H}{\delta n(r)} + \frac{\delta E_{XC}}{\delta n(r)} \right] \frac{\delta n(r)}{\delta \varphi_i^*(r)} - \sum_{ij} \lambda_{ij} \varphi_j(\vec{r}) \quad (2.34)$$

$$\begin{aligned} 0 &= \left( -\frac{1}{2} \nabla^2 + U_{ext} + U_H + U_{xc} - \lambda_i \right) \varphi_i(\vec{r}) \\ 0 &= \left( -\frac{1}{2} \nabla^2 + U_{eff} - \varepsilon_i \right) \varphi_i(r) \\ \left( -\frac{1}{2} \nabla^2 + U_{eff} \right) \varphi_i(\vec{r}) &= \varepsilon_i \varphi_i(\vec{r}) \end{aligned} \quad (2.35)$$

The Lagrange multiplier  $\lambda_{ij}$  is identified as energies of each orbital by diagonalization with unitary transformations of  $\varphi_i(\vec{r})$  or it can be replaced by  $\varepsilon_i$ . The three energy functionals  $E_{ext}, E_H, E_{XC}$  are transformed to their corresponding potentials by these derivative operations and this leads to a set of coupled KS equations in the form of Schrödinger equations with corresponding Hamiltonian  $\hat{H}_{KS}$ , that is (2.35) becomes

$$\hat{H}_{KS} \varphi_i(\vec{r}) = \varepsilon_i \varphi_i(\vec{r}) \quad (2.36)$$

With this the density governing model of DFT is complete. For actual system are performed on this auxiliary Hamiltonian  $\hat{H}_{KS}$  and it require to solve this set of KS equations simultaneously [10] [8] [11].

### 2.6.6.1. KS non-interacting electrons

In the KS approach, the Hamiltonian operator for one electron moving in an average potential is caused by a fictitious system of electrons, in reality the wavefunction of the interacting and non-interacting electrons are different. So, KS method focus on finding the fictitious system of non-interacting electrons which has the density same as the real one with the interacting electrons.

This one-electron reformulation is in fact an excellent approximation of the real N-electron system. The KS orbitals and its energies only correspond to fictitious set of independent electrons.

### 2.6.6.2. KS orbitals and KS eigenvalues

The KS orbitals  $\varphi_i(\vec{r})$  are the solution of the KS equations (2.36, 2.35). For example, a single atom with  $n$  electrons, a set of  $\frac{n}{2}$  KS orbitals will result in the solution if all the orbitals are filled with two electrons. they calculate the noninteracting kinetic energy exactly and generate the electron shell structure of atoms, all in the framework of DFT.

The eigen values  $\varepsilon_i$  could be considered as Lagrange multipliers with no particular physical meaning, they simply represent the energies of each KS electrons and their sum becomes the total energy after double counted errors are removed and qualitatively describe band structure, density of states, bonding character and so on.

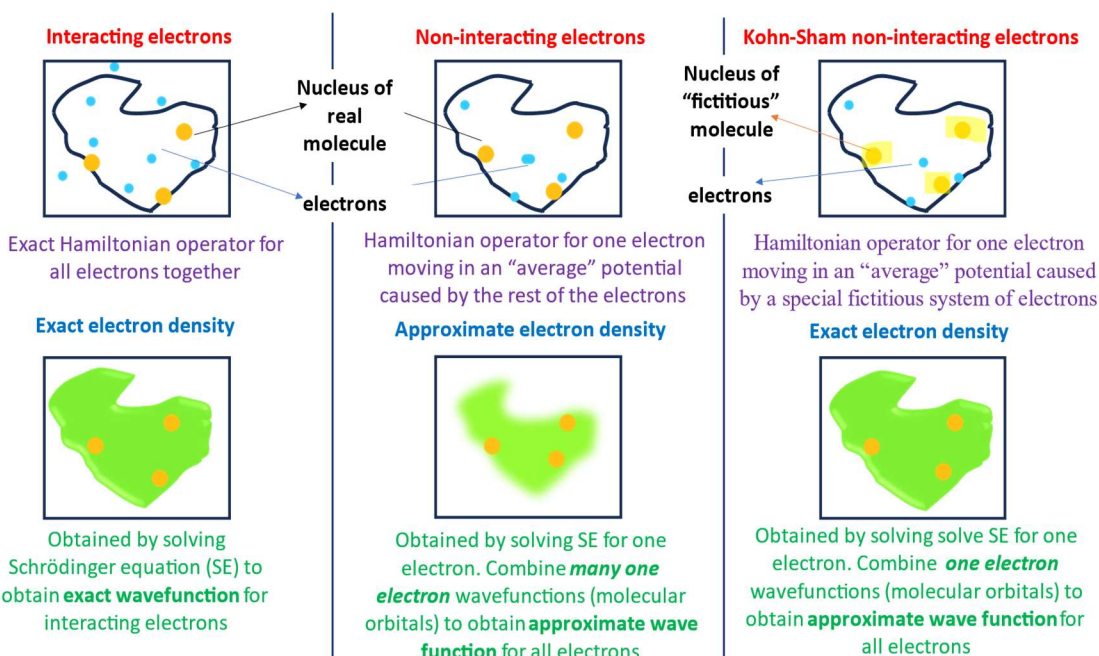


Fig 2.5: Schematic diagram of KS theory of DFT involving fictitious system of electrons

## 2.7. Exchange correlation functional

Up to now we have obtained the KS equations and it should be practically possible to perform self-consistent calculations. However, the major problem is that the exchange-correlation energy  $E_{xc}$  is unknown. Therefore, appropriate approximations are essential.

It is important to find the  $E_{xc}$  because it determined the error involved in the DFT calculation. Normally, this energy is less than approximately 10% of the total energy, but it actively involves determining materials properties, such as bonding, spin-polarization, and band gap formation. As the name indicates, the XC energy represents the lively activities of electrons among one another. Thus, it is necessary to approximate this energy as exactly as possible. The quality of a DFT run is critically determined by how closely the approximate XC energy reproduces the exact value.

### 2.7.1. Local density approximation (LDA)

The basic idea in LDA is to assume a system to be homogenous distribution of electrons locally. That is the complex system can be transformed into many pieces of uniform electron density with different values. It is now possible to calculate the XC energy for each electron with the electron density that is assumed to be constant in that piece and the energies associated with these local elements can be summed up to equal the total XC energy. Thus the  $E_{xc}$  can be written as

$$E_{xc}^{LDA}[n(\vec{r})] = \int \varepsilon_{xc} [n(\vec{r})] n(\vec{r}) d^3\vec{r} \quad (2.37)$$

Were,

$$\varepsilon_{xc}[n(\vec{r})] = \varepsilon_{xc}^{hom}[n(\vec{r})] = \varepsilon_x^{hom}[n(\vec{r})] + \varepsilon_c^{hom}[n(\vec{r})] \quad (2.38)$$

Where, the Exchange energy of the homogeneous gas  $\varepsilon_x^{hom}[n(\vec{r})]$  can be obtained by an analytical form in the HF approximation

$$\varepsilon_x^{ho} [n] = -\frac{0.458}{r_s} \quad (2.39)$$

Where the  $r_s$  is the radius of the sphere enclosing an electron.

The correlation energy of the homogeneous electron system is approximated to good accuracy by the Monte Carlo simulations of Ceperly and Alder [12] as

$$\varepsilon_c^{hom}[n] \approx \frac{0.44}{r_s + 7.8} \quad (2.40)$$

Considering that actual systems are far from the homogeneous electron gas, the LDA works fairly well where the charge density varies relatively slowly, such as in covalent systems and simple metals. It is because LDA fulfils the correct sum rule for the exchange-correlation hole.

The main problems with LDA are it Underestimates the lattice parameters and thus overestimates the cohesive energy and bulk modulus of solids. Calculates the adsorption energies too high and the diffusion barriers too low. Underestimates the spin and orbital moments. Calculates the band gaps  $\sim 50\%$  smaller (e.g., Si) or even no gap (e.g., Ge) and it does not work well for materials that involve weak hydrogen bonds or van der Waals attraction (mainly in atoms and molecules) [13] [12].

### 2.7.2. Generalized gradient approximation (GGAs)

Real systems are evidently not homogeneous and have varying density landscape around electrons. To generate more accurate XC functionals, the GGA captures both the local and semi local information that is the electron density and its gradient at a given point.

Unlike  $E_{xc}^{LDA}$ , there is no simple functional form that correctly represents the GGA data, and thus the function  $E_{xc}^{GGA}$  is often expressed with a properly chosen form and is fitted to satisfy various physical constraints. Therefore, the general form of GGA in practice is expressed based on the LDA with an additional enhancement factor  $F(s)$  that directly modifies the LDA energy.

$$E_{xc}^{GGA}[n(\vec{r}), s] = \int \varepsilon_{xc}^{GGA}[n(\vec{r})] n(\vec{r}) F(s) d\vec{r} \quad (2.41)$$

Here,  $s$  depends on both electron density and its gradient

$$s = C \frac{|\nabla n(\vec{r})|^{\frac{4}{3}}}{n^{\frac{5}{3}}(\vec{r})} \quad (2.42)$$

In solids, the typical range of  $s$  is  $= 0\text{--}3$ . Many different forms of GGA have been proposed, and the popular choices are PW91 and PBE [14].

### 2.7.3. Perdew, Burke and Ernzerhof (PEB) approximation

PBE presents a simplified and improved GGA version with no empirical elements. It includes features such as local electron density and its gradient and second-order gradient in the enhancement factors,  $F(x)$  and  $F(c)$ . In PEB approximation  $E_{xc}$  can be written as

$$E_{xc}^{PEB}[n(\vec{r}), s, c] = \int \varepsilon_{xc}^{GGA} [n(\vec{r})] n(\vec{r}) F(s, c, r_s) d^3\vec{r} \quad (2.43)$$

Where,  $s$  is the density gradient,  $c$  is the spin-polarization,  $r_s$  is the local Seitz radius. The enhancement factor  $F(s, c, r_s)$  keeps the features of LDA and includes the inhomogeneity contributions. The PEB contribution is employed in the following calculations because of its improves descriptions of bond lengths and bond angles [14].

A revised version of PBE (Zhang and Yang 1998) is also available, namely, revPBE. It differs only slightly from the PBE functional as a simpler mathematical form for  $\varepsilon_{xc}^{GGA}$ . This functional is known to give better results when adsorption or hydrogen bonding is involved.

#### 2.7.4. Other XC functionals

If one can afford at least a 10-fold increase in computational cost, one may go for one of the advanced functionals beyond common GGAs. Advance functionals (PBE0, meta-GGA, hyper-GGA, HSE, hybrid functional such as B3LYP, etc.) claim better accuracies, reporting successive improvements in energetics. They incorporate with additional variables (for example, higher-order density gradient) or mixing a certain amount of nonlocal HF exchange energy.

The hybrid functionals are, as the name suggests, GGA-type functionals combined with some (~25%) of the accurate exchange energy from the HF method. Remember that the HF method does not account for the correlation energy that causes spatially closer electrons, smaller bond length, larger binding energy, wider band gap, and thus higher energy. In the DFT, on the other hand, systematic errors occur in the opposite way. Thus, it is expected that the DFT exchange energies can reduce the errors if one introduces the HF exchange energy into  $\varepsilon_{xc}$ , typically in the form of

$$E_{xc} = CE_x^{HF} + (1 - C)\varepsilon_{xc}^{GGA} + E_c^{GGA} \quad (2.44)$$

The B3LYP functional has been developed and upgraded by a group of scientists for many years (Stephens et al. 1994). It is a three-parameter functional fitted to atomization energies, ionization potentials, and so on. It is now very popular, especially in the field of molecular chemistry.

This hybrid functional can describe systems even with rapid variations in electron density or with long-range interaction such as the van der Waals type. It is generally best suited for calculations of bond energies, chemical transition-state barriers, band gap, and so on. These advanced functionals are often contaminated with empirical elements, losing the

first-principles origin. And the claimed improvement could be a system-dependent result. In addition, since so many XC functionals are available, it is sometimes a concern that someone may choose the XC functional that gives the result that one wants to have. One should not just jump into a new functional even if it produces more accurate numbers for a system, unless all aspects are carefully considered and justified [10] [6].

# CHAPTER 3

## Tools and techniques

### 3.1. The plane wave basis set

In Quantum chemical calculations, a basis set is a collection of functions, referred to as basis functions. These functions are utilized to express the electronic wave function within the frameworks of the HF method or DFT. The purpose is to transform the model's partial differential equations into algebraic equations, making them suitable for efficient computer implementation.

Within the basis set, the wavefunction is represented as a vector, the components of which correspond to coefficients of the basis functions in the linear expansion. In such a basis, one-electron operators correspond to matrices (a.k.a. rank two tensors), whereas two-electron operators are rank four tensors. The use of basis set is equivalent to the use of an approximate resolution of the identity that is the orbitals are expanded within the basis set as a linear combination of basis functions. There are various basis set like linear combination of atomic orbitals (LCOA), plane waves (PW), Gaussian wave (GW), Slater orbitals, numerical orbitals, linearized augmented-plane wave basis (LAPW) set and more. In this thesis the PW basis set is employed to perform the calculations [15].

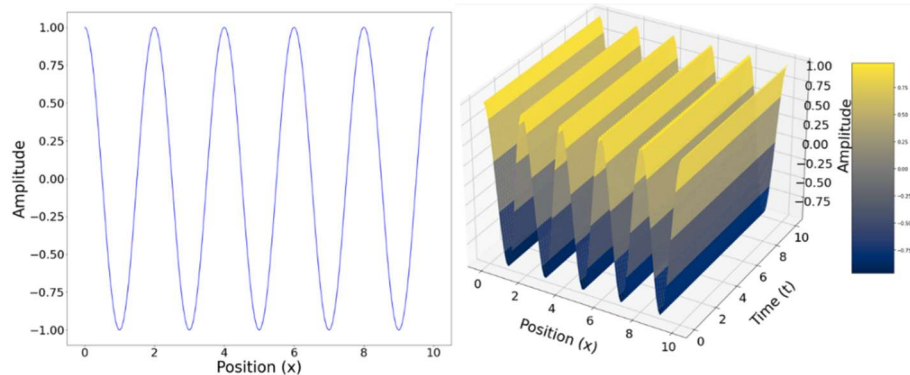


Fig3.1: Representation of planewaves in 2D and 3D space

#### 3.1.1. Periodic systems and Bloch's theorem

Any repetitive and periodic distribution of a set of objects can be described, by translations that repeat the set of objects periodically. The implied translations generate a direct lattice (or real lattice) in the real space  $\vec{r}$  and the lattice vectors are given as  $\vec{R}$ . The translations that describe the periodicity in crystals can be expressed as a linear combination of three basic translations which are independent, known as lattice axes (or unit cell axes).

These axes define a parallelogram in 2D, or a parallelepiped 3D known as a unit cell. This elementary area, or elementary volume which holds the minimum set of the periodic distribution, generates the full distribution which, in the 3D atomic case is called a crystal. The system of axes defining the unit cell defines the reference system to describe the positional coordinates of each atom within the cell. In general, inside the unit cell there is a minimum set of atoms (ions or molecules) which are repeated inside the cell due to the symmetry elements of the crystal structure. This minimum set of atoms (ions or molecules) which generate the whole contents of the unit cell after applying the symmetry elements to them is known as the asymmetric unit [6].

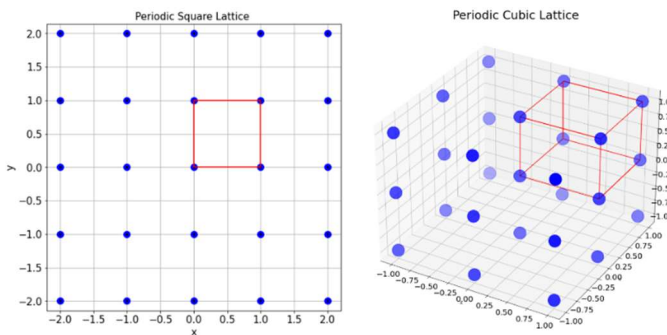


Fig 3.2: Representation of periodic lattice in 2D and 3D where the unit cell is highlighted in red, the unit cell size in 1 atomic unit and the blue dots represents the lattice points.

Reciprocal space emerges from the Fourier transform from the real space. The reciprocal lattice exists in the mathematical space of spatial frequencies, known as reciprocal space  $\vec{k}$  which is nothing but the wavevector and the lattice vector is represented by  $\vec{G}$ . The real space lattice describes the periodic structure and the reciprocal lattice determines how the periodic structure interacts with waves [8].

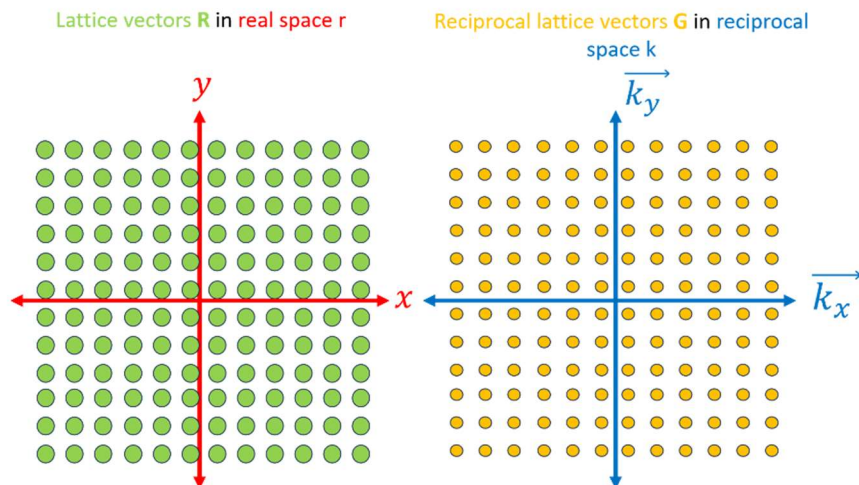


Fig 3.3: Representation of lattice vectors in real space and reciprocal space where the spacing of  $\mathbf{R}$  is inversely proportional to  $\mathbf{G}$

Periodic boundary conditions (PBCs) are a set of boundary conditions that are used for approximating a large system by a small part called a unit cell. The large systems approximated by PBCs consist of an infinite number of unit cells. In computer simulations, one of these is the original simulation box, and others are copies called images. During the simulation, only the properties of the original simulation box need to be calculated, which is then expanded for the whole system.

A crystalline solid consists of a huge number of atoms in the order of  $6.022 \times 10^{23}$ . In this case the number of atoms and electrons are considered to be infinite. This big system can be represented by a unit cell or a Wigner-Seitz cell which keeps all the crystal information of the corresponding crystalline structure. The unit cell generally contains a few atoms and it is periodically repeated through space.

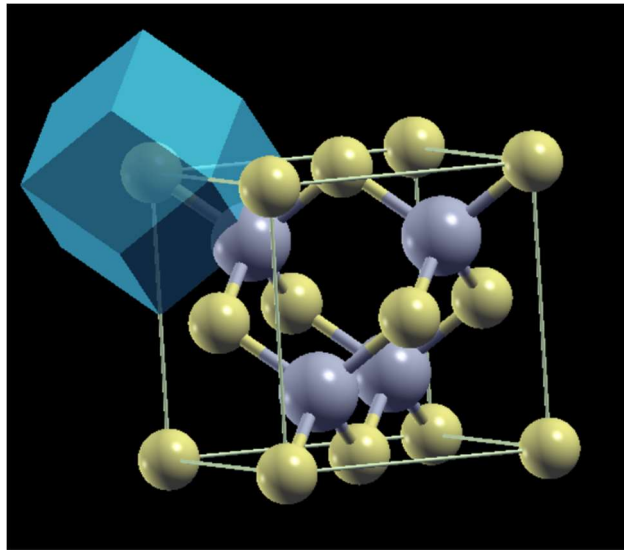


Fig 3.4: Wigner-Seitz of ZnS viewed using XCrySDen

Bloch's theorem helps us to exploit electrons in periodic infinite system to those in unit cell. According to this theorem, the wave functions of electrons in a periodic potential, in this case KS potential, can be written as a product of periodic function and the plane wave [6].

$$\psi_{\vec{k}}(\vec{r}) = \exp[i\vec{K} \cdot \vec{r}] u_{\vec{k}}(\vec{r}) \quad (3.1)$$

Where  $u_{\vec{k}}(\vec{r})$  is the cell periodic function such that

$$u_{\vec{k}}(\vec{r}) = u_{\vec{k}}(\vec{r} + \vec{R}) \quad (3.2)$$

for all lattice vectors  $\vec{R}$ . This implies that

$$\psi_{\vec{k}}(\vec{r} + \vec{R}) = \exp[i\vec{K} \cdot \vec{R}] u_{\vec{k}}(\vec{r}) \quad (3.3)$$

and  $\vec{K}$  is the wave vector which is used to describe the wavefunction as an envelope of waves. As for all lattice-periodic functions only certain plane waves will appear in the Fourier expansion of  $u_{\vec{k}}(\vec{r})$

$$u_{\vec{k}}(\vec{r}) = \frac{1}{\Omega} \sum_{\vec{G}} C_{\vec{k}\vec{G}} \exp(i\vec{G} \cdot \vec{r}) \quad (3.4)$$

### 3.1.2. The plane wave expansion

The main logic of the plane wave expansion is assemblies of atoms are considered as slight distortions to free electrons [8]. The system under consideration is assumed to be placed inside a unit cell defined by the unit vectors  $\vec{a}_1, \vec{a}_2, \vec{a}_3$  with unit cell volume

$$\Omega = [\vec{a}_1, \vec{a}_2, \vec{a}_3] = \vec{a}_1 \cdot (\vec{a}_2 \times \vec{a}_3) \quad (3.5)$$

The plane waves given by (3.4) in this expansion is represented as a grid in K-space (also called as FFT Grid) [16], which is discrete only for true periodic systems and in principle infinite number of plane waves are required. Since the system is periodic in nature the PW expansion (3.4) must consist of only the plane-waves  $\exp(i\vec{G} \cdot \vec{r})$  that have the periodicity of the lattice, such type of PW waves can be obtained from the following constraint

$$\exp(i\vec{G} \cdot \vec{r}) = \exp i\vec{G}(\vec{r} + \vec{R}) \quad (3.6)$$

The smallest  $\vec{G}$  is given by the largest wavelength in the real space hence it is always discrete

$$\vec{G}_{min} = \frac{2\pi}{2a} \quad (3.7)$$

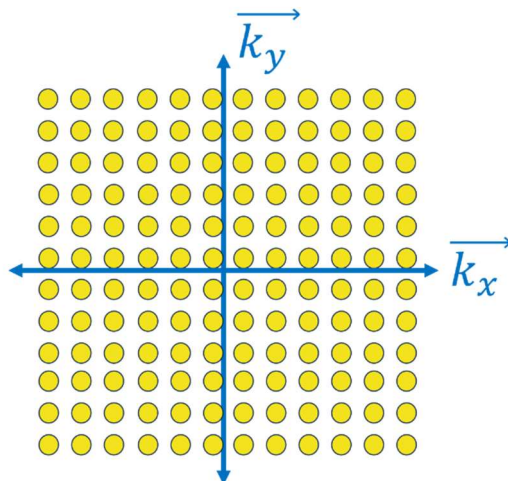


Fig 3.5: The FFT grid of (12 x 12 x 1). The plane waves that appear in this expansion can be represented as a grid in k-space

### 3.1.3. Truncating the PW expansion (Wavefunction cutoff energy)

In practice the contribution from higher Fourier components is small and the PW is expanded infinity truncating it using a cut-off energy will improve the computation speed, Thus the wave-function cut-off is given as

$$E_{cut} = \frac{\hbar^2}{2m} |\vec{G}_{max}|^2 \quad (3.8)$$

The cut-off energy is not only for the wavefunction in general but the orbitals and the charge density can also be represented using the cut-off energy

$$E_{cut \text{ of charge density}} = 4 E_{cut \text{ of orbitals}} \quad (3.9)$$

Normally twice maximum grid dimension is to store charge density as orbitals [16].

The cut-off energy is a key convergence parameter. Larger values always correspond to better results but need more computer time and memory. The ground state energy obeys variational principle and hence increasing  $E_{cut}$  adds more variational freedom and hence monotonically improves the quality of the density and lowers the ground state energy [8] [17].

The  $E_{cut}$  in (3.8) is usually represented as

$$E_{cut} \geq \frac{\hbar^2}{2m} |\vec{k} + \vec{G}|^2 \text{ and } |\vec{k} + \vec{G}| < \vec{G}_{max} \quad (3.10)$$

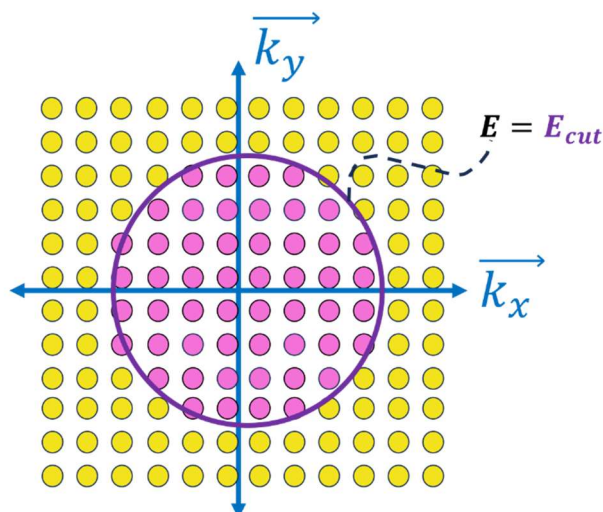


Fig 3.6: Representation of PW cutoff energy

### 3.1.4. K-points and sampling the first BZ

From the Bloch's theorem (3.1) it is seen that in a periodic potential the wavefunction is quasi-periodic i.e. the neighbouring cells vary by a phase factor hence it is necessary to integrate over all possible  $\vec{k}$  values while constructing the density

$$n(\vec{r}) = \int |\varphi_{\vec{k}}(\vec{r})|^2 d^3\vec{k} \sim \sum_{\vec{k}} |\varphi_{\vec{k}}(\vec{r})|^2 \quad (3.11)$$

The sampling of  $\vec{k}$ -points is done within the 1<sup>st</sup> Brillouin zone (BZ) and the number of finite k-points depends on the size of BZ. In case of insulators due to having filled bands a few k-points is enough but for metals more k-points are required to describe the bands near the fermi surface where fermi factor changes rapidly. Generally, the sampling is done using the Monkhorst-Pack mesh, which is based on the equally-spaced grid determined by a formula

$$\vec{k}_{n_1, n_2, n_3} = \sum_i^3 \frac{2n_i - N_i - 1}{2N_i} \vec{G}_i \quad (3.12)$$

Higher number of K-points lead to convergence of total energy, this can be computationally costly but can be reduced using the crystal symmetry and it is required to choose a k mesh which leads to convergence [18].

## 3.2. Pseudopotentials (PPs)

The steep ionic potential

$$V(\vec{r}) = -\frac{Ze}{r} \quad (3.13)$$

Near the ion causes rapid oscillations of  $\varphi_{\vec{k}}(\vec{r})$ . Apart from this the valence electrons are strongly affected by the Coulomb potential this causes an orthogonality constraint to the core orbitals. In such a case the Fourier components need very high energy PW cut-off. Practically the filled core electrons are unperturbed by crystalline environment. So, all the chemical interaction only take place through the valence electrons.

Therefore, to reduce the computational cost and time the Pesudopotential approximation is introduced. Pseudopotentials, also known as "effective potentials" or "model potentials," are a concept primarily used in quantum mechanics, particularly in the study of atoms, molecules, and solid-state physics. Pseudopotentials offer a way to simplify the calculations by effectively removing the highly localized inner electron states from the

problem, which don't significantly contribute to the bonding and chemical properties of the system being studied. Pseudopotentials achieve this by replacing the true potential that electrons experience in the presence of atomic nuclei with an approximate potential that retains only the long-range behaviour and essential features of the true potential. This allows for a substantial reduction in the computational cost while still providing accurate results for many properties of interest [8].

There are different types of pseudopotentials used depending on the application and level of accuracy required. Norm-conserving pseudopotentials (NC PPs) maintain the norm of the wave function (probability conservation), while ultrasoft pseudopotentials (UPF PPs) are more flexible and can represent the potential with fewer basis functions, allowing for further computational savings, both the types are implemented in the following calculations in which the UPF file format is used which is one of the inputs to the electronic structure calculation code [19] [20].

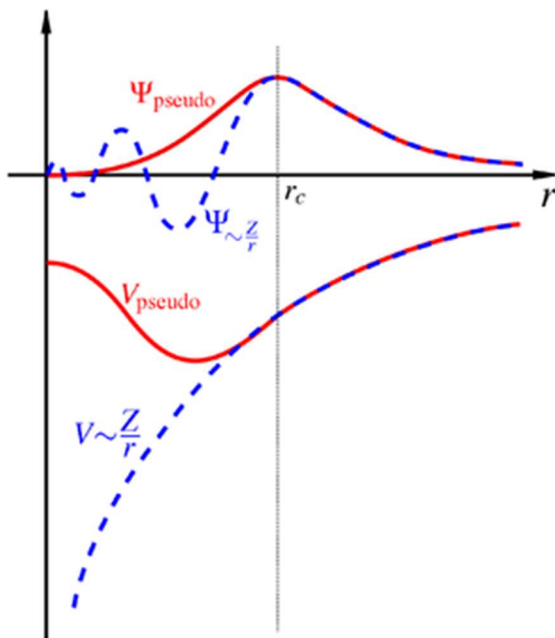


Fig 3.7: Comparison of a wavefunction in the Coulomb potential of the nucleus (blue) to the one in the pseudopotential (red). The real and the pseudo wavefunction and potentials match above a certain cutoff radius [21].

The term "soft" indicates that the pseudopotential has been constructed in a way that allows it to be more flexible or less rigid compared to other types of pseudopotentials. The softness of a pseudopotential refers to how smoothly and accurately it approximates the true potential experienced by the valence electrons near the nucleus. Soft pseudopotentials achieve this smoothness by allowing more flexibility in the construction of the pseudopotential function. This flexibility often involves using a larger basis set or introducing additional

parameters in the construction of the pseudopotential, which can improve the accuracy of the approximation while maintaining computational efficiency. By providing a more accurate description of the atomic interactions, soft pseudopotentials can lead to more reliable and accurate predictions of the electronic and structural properties of materials [14].

### Constructing a PPs file

Step 1: Solve all-electron eigenvalues and wavefunctions for a reference atom,

Step 2: Construct pseudo wavefunction from the all-electron wavefunctions, such that:

- Real and pseudo eigenvalues agree.
- Real and pseudo atomic valence wavefunctions agree beyond a chosen “core radius”  $r_c$
- Real and pseudo valence charge densities agree for  $r > r_c$
- Logarithmic derivatives and the first energy derivatives agree for  $r > r_c$

Step 3: Invert the atomic Schrödinger Equation to obtain a screened pseudopotential.

Step 4: Generate an ionic pseudopotential from the screened pseudopotentials.

Step 5: Transform the semi-local potential to a non-local form (Kleinman-Bylander).

Thus, using PPs can be considered as Frozen core approximation in which the core-electrons degrees freedom is removed and the calculation becomes “Naot an all electron”.

### 3.3. Units used in DFT

The atomic units are introduced in order to reduce the equations. Atomic units are a set of units of measurement that are especially convenient when dealing with atomic-scale phenomena, such as those encountered in quantum mechanics and electronic structure calculations [22]. The atomic units are used for the following reasons

- **Natural Scaling:** Atomic units are scaled in such a way that fundamental physical constants like the electron charge ( $e$ ), electron mass ( $m_e$ ), and Planck's constant ( $\hbar$ ) are set to unity. This simplifies many of the equations in DFT, as these constants frequently appear and setting them to 1 reduces clutter and simplifies calculations.
- **Atomic Scale:** DFT often deals with systems at the atomic scale, such as atoms, molecules, and solid-state materials. Using atomic units allows for a more intuitive

understanding of the quantities involved, as they are tailored to the scale of these systems.

- **Reduced Complexity:** Expressing quantities in atomic units eliminates the need for conversion factors involving physical constants. This simplifies calculations and reduces the likelihood of errors.
- **Consistency:** When working within the framework of DFT, many of the equations and theoretical concepts are naturally expressed in terms of atomic units. Using atomic units ensures consistency throughout the calculations and facilitates comparison between different systems and methods.

The atomic units used are defined as follows

- Length: The unit of length is the Bohr radius ( $a_0$ ),

$$1 a_0 \approx 0.52918 \times 10^{-10} \text{ meters.}$$

- Energy: The unit of energy is the Hartree (Ha), which is equivalent to the energy of one electron when it is in the ground state of a hydrogen atom.

$$1 \text{ Hartee} = 27.2114 \text{ eV}$$

- Rydberg unit of energy, symbol Ry, corresponds to the energy of the photon whose wavenumber is the Rydberg constant, i.e. the ionization energy of the hydrogen atom in a simplified Bohr model.

$$1 \text{ Ry} = 13.605693122944 \text{ eV}$$

- Mass: The unit of mass is the electron mass ( $m_e$ ).
- Charge: The unit of charge is the elementary charge ( $e$ ).
- Time: The unit of time is derived from the other units to ensure that constants like the speed of light in vacuum ( $c$ ) and Planck's constant ( $\hbar$ ) are equal to unity.

### 3.4. Quantum ESPRESSO (QE) code

Quantum ESPRESSO (QE) is an open-source software suite for electronic structure calculations and materials modelling based on density functional theory (DFT). It offers a comprehensive set of tools for simulating the properties of materials at the atomic scale, including atoms, molecules, and solid-state systems. QE provides a range of functionalities from the ground state calculation, structural optimization, electronic structure analysis to calculating optical properties and phonon calculations [23].

In this work, QE is employed to perform electronic structure calculations on organic and inorganic materials which have potential application in NLO and THz generation. Ground-state calculations were carried out to determine the total energy and electronic structure of the system. Structural optimization was performed to find the equilibrium atomic positions and lattice parameters. Additionally, optical calculations is conducted to investigate the absorption spectra of the materials.

The following simulation parameters which were discussed in above sections are used in the QE calculations:

- Exchange-Correlation Functional: Perdew-Burke-Ernzerhof (PBE), Generalized Gradient Approximation (GGA).
- Plane-wave Energy Cutoff
- K-Point Sampling
- Pseudopotentials: The PseudoDojo NC SR PPs v0.5 with PBE XC and stringent accuracy in .UPF format is used.
- Convergence Criteria: Describe the convergence criteria used for self-consistent field calculations, structural optimizations, etc.

In the PWscf – Paane wave self-consistent field package is used for the calculation of electronic properties and the geometry optimization. Apart from it the XSPECTRA and TDDFT (Time dependent density functional theory) is used to calculate the absorption spectra using the Coupled linear-response TDDFT equations and quantum Liouville equation using Lanczos algorithm. Finally, the BURAI (QE GUI) is used to visualize the structures and modify the input files.

### 3.4.1. The QE SCF Iterative solution

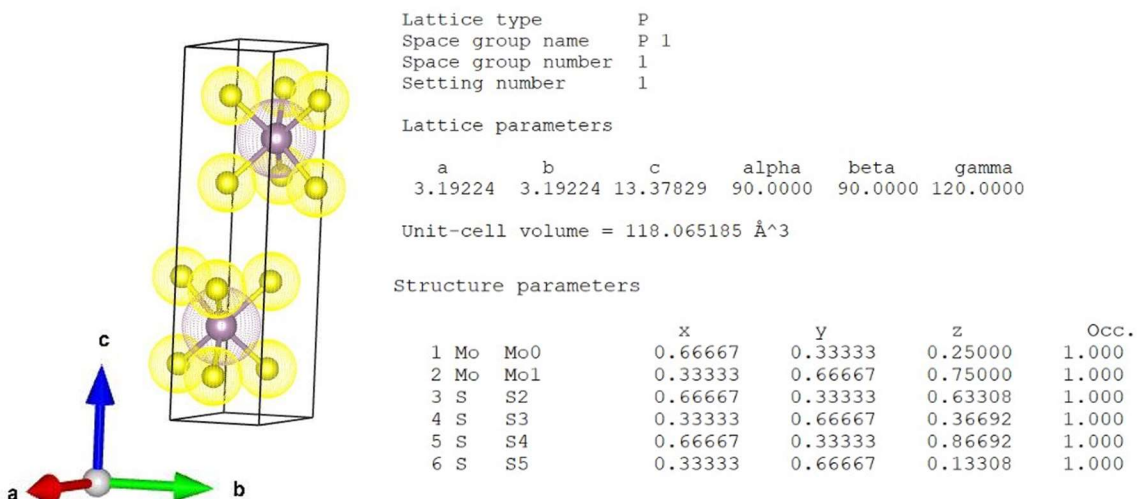


Fig 3.8: The MoS<sub>2</sub> system and its structural parameters.

The SCF loop is used to solve the KS equations for a set of fixed ionic positions. The SCF method described in section 2.5 is used here with the KS equations and charge density [24].

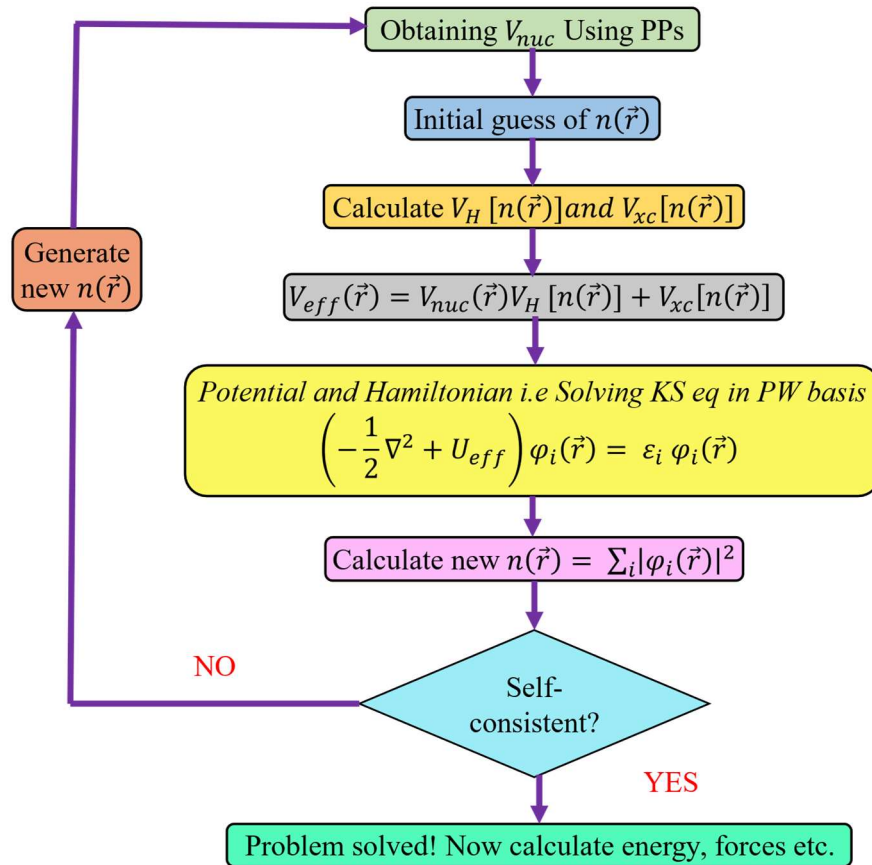


Fig 3.9: Flow chart representing the SCF loop

### 3.4.2. Parameters for QE input file for SCF calculation

The first step is to define the periodic system. Using the *namelist* ‘SYSTEM.’ All periodic systems can be specified by a Bravais lattice and an atomic basis [25].

- The ‘ibrav’ defines the type of Bravais lattice there are 20 different system from which we can selected them and each Bravais lattice can be described by a number. For example, 8 represents the Orthorhombic P structure. Even non primitive unit cells are available.
- For the selected ‘ibrav’ corresponding ‘celldm(i)’ is given which represents lattice vectors or instead of ‘celldm(i)’, **A**, **B**, **C**, **cosAB**, **cosAC**, **cosBC** can be used to describe the dimension od lattice vectors.
- The number of atoms in the unit is described by ‘nat’ and the number of different types of elements is described by ‘ntyp’. Both of these parameters take a positive number as input.

- The number of electronic states (bands) to be calculated is described by ‘**nbnd**’. For insulator it is equal to the number of valance bands which is  $\frac{\text{no. of electrons}}{2}$  and for metals it is 20% more than this.
- The total charge of the system for simulations with charged cells is given by ‘**tot\_charge**’ which is take a real number as input.
- The total majority spin charge - minority spin charge. Which is used to impose a specific total electronic magnetization is described by ‘**tot\_magnetization**’ If unspecified then tot\_magnetization variable is ignored and the magnetization is not taken into account during the self-consistent cycle.
- The kinetic energy cutoff for the wavefunctions (3.8) in Ry units given by ‘**ecutwfc**,’ any real number can be given as input. This can be calculated analytically by considering the charge density of the system and the size of the system. Generally higher value will make the calculation more accurate but it increases the computational space.
- Kinetic energy cutoff (Ry) for charge density and potential is described by ‘**ecutrho**.’ For NC PPs one should stick to the default value, reducing it by a little but it will introduce noise especially on forces and stress. If there are ultrasoft PPs, a larger value than the default is often desirable (ecutrho = 8 to 12 times ecutwfc, typically). PAW datasets can often be used at 4\*ecutwfc. The 3D FFT mesh (hard grid) for charge density (and scf potential) ‘nr1, nr2, nr3’ and 3D mesh for wavefunction FFT and for the smooth part of charge density (smooth grid) ‘nr1s, nr2s, nr3s’ is calculated from ecutrho and ecutwfc.
- ‘**nosym**’ is a logical parameter (. true or . false) which gives the option to calculate the system with low-symmetry large cells and isolated atoms. If not used properly this can cause problems in memory segmentation.
- The occupations of the atoms are described by the ‘**occupations**’ parameter which takes input as a character. The following occupations are widely used.
  - ‘smearing’ - in which the occupied states of the KS system is smooth according to a smooth function like a Fermi distribution. Usually, it is applied for metals and a gaussian smearing is used. The gaussian spreading in Ry units for the BZ integration in metals is given by the ‘degauss’ parameter which takes a real value as input.
  - ‘fixed’ – is used for insulators with gap.

- The polarization parameters are described by the ‘**nspin**’ parameter which has three values each represent a type of spin-polarization calculation.
  - 1: non-polarized calculation (default)
  - 2: spin-polarized calculation, LSDA (magnetization along z axis)
  - 4: spin-polarized calculation, noncollinear
- The XC functional and other external energy is given as input to the QE code using the PPs by the ‘**input\_dft**’ parameter.

The next step is to define the parameters of electrons and convergence system. Using the *namelist* ‘**ELECTRONS**’. This block controls how the calculation is performed. Iterative diagonalization is used, and both the charge density and wavefunctions are improved towards the “true” solution.

- The convergence threshold is described by the parameter ‘**conv\_thr**’. This means that self-consistency is achieved when the energy changes by less than  $10^{-8} \text{ Ry}$  in each cycle it is a conventionally chosen value.
- The method for diagonalizing the Kohn-Sham Hamiltonian is given by the parameter ‘**diagonalization**’. In general, the Davidson iterative diagonalization with overlap matrix is used due to its fast implementation.
- The mixing method of the system is described by the parameter ‘**mixing\_mode**’. This describes how the charge density is changed (mixed) from step to step towards self-consistency. By default the plane mode is used apart form it the Thomas-Fermi(TF) mode and the local-TF mode can be used.
- The starting wavefunction is described by the parameters ‘**startingpot**’ and ‘**startingwfc**’. Both of them take the input as characters. The startingpot represents from where the starting potential is calculated, there are two options available ‘atomic’ where the starting potential is from the atomic charge densities which is default for scf or from ‘file’ i.e. the starting potential is calculate from the cherge\_density.xml file it is default for nsdf and band calculations. The startingwfc describes how the wavefunction is developed using the potentials, atomic + random is the default i.e. it Start from superposition of atomic orbitals. If enough atomic orbitals are now available, fill with random numbers the remaining wfcs. The scf typically starts better with this option, but in some high-symmetry cases one can "loose" valence states, ending up in the wrong ground state plus a superimposed "randomization" of atomic orbitals. Prevents the "loss" of states.

The next step is to define the atoms present in the system. Using the *namelist* ‘**ATOMIC\_SPECIES**’. This block contains the details of each ntype and the PP file path.

- "atomic-symbol", "atomic-weight", "pseudo-potential.upf"
- The pseudo-potential is the name of a file in ‘\pseudo\_dir’

The next step is to define the atomic positions in the system. Using the *namelist* ‘**ATOMIC\_POSITIONS**’. This block gives the atomic positions in Alat, Bohr, Crytal or Armstrong for each nat.

- atomic-symbol x y z – where x, y, z are given in the units specified by units.

The next step is to define the k-point mesh (FFT grid). Using the namelist ‘**K\_POINTS**’ of the system is defined. Which is essentially the BZ sampling

- ‘tpiba OR crystal OR tpiba\_b OR crystal\_b OR tpiba\_c OR crystal\_c’ is used to define the k-points for the band calculation and other calculations.
- For SCF calculation the ‘automatic’ option is chosen, which generates the k-mesh according to the system.
- In the case of automatic generation, the next line is – nkx nky nkz offx offy offz – where nk is the number of intervals in a direction and off is the offset of the origin of the grid.

### 3.5. The control block of QE

The **CONTROL** namelist of the QE pw.x executable is the block which defines which type of calculation should be performed, where the outfiles and the log files must be stored, defined the mode of calculation and the number of iterations for SCF calculations [25].

- The parameter ‘**calculation**’ defines which calculation is performed among ‘scf’, ‘nscf’, ‘bands’, ‘relax’, ‘md’, ‘vc-relax’ and ‘vc-md’.
- The **title card** provides the title of the system for which the calculation is performed.
- The parameter ‘**restart\_mode**’ defines how the calculation should be performed if the same calculation is repeated. ‘from\_scratch’: From scratch. This is the normal way to perform a PWscf calculation ‘restart’: From previous interrupted run. Use this switch only if you want to continue, using the same number of processors and parallelization, an interrupted calculation. Do not use to start a new one, or to perform a non-scf calculations.

- The parameter ‘**nstep**’ defines the number of iterations to be performed in a SCF or NSCF calculation.
- The parameters ‘**tstress**’, ‘**tprnfor**’ are included to calculate the stress and the force in md and relax calculation upon convergence.
- The ‘**outdir**’ parameter specifies the directory to store the cache and temporary file of the calculations.

### 3.6. The QE input file

The QE input file is usually written in notepad and used as a INPUT file that is a .in file.

```
&CONTROL
  calculation = 'scf'
  restart_mode='from_scratch'
  prefix = 'TaAs'
  outdir = './outdir'
  pseudo_dir = '/home/johnpaul/JP_QME/Dojo_Pseudo/nc-sr-
05_pbe_stringent_upf'
/
&SYSTEM
  a          = 3.44363e+00
  c          = 1.17359e+01
  degauss    = 1.00000e-02
  ecutrho    = 2.25000e+02
  ecutwfc   = 2.50000e+01
  ibrav     = 6
  nat        = 8
  nspin      = 2
  ntyp       = 2
  occupations = "smearing"
  smearing   = "gaussian"
/
&ELECTRONS
  conv_thr      = 1.00000e-06
  electron_maxstep = 200
  mixing_beta    = 4.00000e-01
  startingpot    = "atomic"
  startingwfc   = "atomic+random"
/
K_POINTS {automatic}
3 3 1 0 0 0

ATOMIC_SPECIES
Ta 180.94790 Ta.upf
As 74.92160 As.upf

ATOMIC_POSITIONS {angstrom}
Ta 0.000000 0.000000 8.801529
Ta 0.000000 1.721813 11.735499
Ta 1.721813 1.721813 2.933587
Ta 1.721813 0.000000 5.867558
As 0.000000 0.000000 3.903732
As 0.000000 1.721813 6.837702
As 1.721813 1.721813 9.771673
As 1.721813 0.000000 0.969761
```

### 3.7. Running the QE package

The QE code contains a huge collection of executables for various calculations. The pw.x executable is mostly used for the scf calculation and electronic calculations [26].

```
johnpaul@LAPTOP-2FES5HJM:~/q-e-qe-7.2$ cd bin
johnpaul@LAPTOP-2FES5HJM:~/q-e-qe-7.2/bin$ ls
average.x      dos.x        kpoints.x      oscdft_pp.x    ppacf.x      pwi2xsf.x
band_interpolation.x epsilon.x    ld1.x       path_interpolation.x pprism.x      rismld.x
bands.x        ev.x        manycp.x      plan_avg.x    projwfc.x    scan_ibrav.x
cell2ibrav.x   fermi_proj.x manypw.x     plotband.x    pw.x         sumpdos.x
cp.x           fermi_velocity.x molecularpdos.x plotproj.x    pw2bgw.x     wannier_ham.x
cppp.x          fs.x        neb.x       plotrho.x    pw2critic.x  wannier_plot.x
d3hess.x       ibrav2cell.x open_grid.x   pmw.x        pw2gw.x     wfck2r.x
dist.x          initial_state.x oscdft_et.x  pp.x        pw2wannier90.x wfdd.x
```

Fig 3.10: Available executables for various calculations

The directory in which the input file \*scf.in) is present is opened and the following command is given to run the pw.x executable for the scf calculation.

```
pw.x <scf.in> scf1.out
```

```
johnpaul@LAPTOP-2FES5HJM:~/JP_QME/OpticalCal/TaAs/dos$ ls
TaAs.dos.dat  TaAs.dos1.dat  TaAs.png  TaAsdos.png  dos.in  dos.out  nscf.in
nscf.out  outdir  scf.in  scf.out
johnpaul@LAPTOP-2FES5HJM:~/JP_QME/OpticalCal/TaAs/dos$ pw.x <scf.in> scf1.out
```

Fig 3.11: Running the pw.x executable for scf calculation

Once the calculation is over the output file and the temporary file are stored in the same directory under the name outdir in which the input file is present.

```
johnpaul@LAPTOP-2FES5HJM:~/JP_QME/OpticalCal/TaAs/dos$ ls
TaAs.dos.dat  TaAs.png  dos.in  nscf.in  outdir  scf.out
TaAs.dos1.dat  TaAsdos.png  dos.out  nscf.out  scf.in  scf1.out
johnpaul@LAPTOP-2FES5HJM:~/JP_QME/OpticalCal/TaAs/dos$ cd outdir
johnpaul@LAPTOP-2FES5HJM:~/JP_QME/OpticalCal/TaAs/dos/outdir$ ls
TaAs.save  TaAs.wfc1  TaAs.xml
```

Fig 3.12: The output file and the files stored in the temporary directory.

### 3.8. The QE output file

The output file contains all the information about the calculation. The following will give the description of the QE output file.

First the k point sampling and the hardware system information along with the G-vector stick and the symmetry operations are provided. The next block contains the structural parameters. Next the PPs information is provided. The atomic positions are given and the memory usage of the calculation is mentioned. The scf loop details are provided till the convergence is achieved.

```

Parallel version (MPI), running on      1 processors

MPI processes distributed on      1 nodes
Waiting for input...
Reading input from standard input

Current dimensions of program PWSCF are:
Max number of different atomic species (ntypx) = 10
Max number of k-points (npk) = 40000
Max angular momentum in pseudopotentials (lmaxx) = 3
Message from routine read_pp_mesh:
mesh size missing, using the one in header
Message from routine read_pp_mesh:
mesh size missing, using the one in header

Subspace diagonalization in iterative solution of the eigenvalue problem:
a serial algorithm will be used

Found symmetry operation: I + ( 0.5000  0.5000 -0.5000)
This is a supercell, fractional translations are disabled

G-vector sticks info
-----
sticks:   dense    smooth      PW      G-vecs:   dense    smooth      PW
Sum        757       341       97       53493     15907     2543

```

Fig 3.13: First block of QE output file.

```

bravais-lattice index      =          6
lattice parameter (alat)  =      6.5075 a.u.
unit-cell volume          =  939.1738 (a.u.)^3
number of atoms/cell      =          8
number of atomic types    =          2
number of electrons        =     200.00
number of Kohn-Sham states= 120
kinetic-energy cutoff     =  25.0000 Ry
charge density cutoff     = 225.0000 Ry
scf convergence threshold = 1.0E-06
mixing beta               = 0.4000
number of iterations used =      8 plain      mixing
Exchange-correlation= PBE
( 1   4   3   4   0   0   0)

celldm(1)= 6.507518 celldm(2)= 0.000000 celldm(3)= 3.408003
celldm(4)= 0.000000 celldm(5)= 0.000000 celldm(6)= 0.000000

crystal axes: (cart. coord. in units of alat)
a(1) = ( 1.000000  0.000000  0.000000 )
a(2) = ( 0.000000  1.000000  0.000000 )
a(3) = ( 0.000000  0.000000  3.408003 )

reciprocal axes: (cart. coord. in units 2 pi/alat)
b(1) = ( 1.000000  0.000000  0.000000 )
b(2) = ( 0.000000  1.000000  0.000000 )
b(3) = ( 0.000000  0.000000  0.293427 )

```

Fig 3.14: Structural parameters in the QE output file.

```

PseudoPot. # 2 for As read from file:
/home/johnpaul/JP_QME/Dojo_Pseudo/nc-sr-05_pbe_stringent_upf/As.upf
MD5 check sum: e06c8bc9a50762e91a9491b3a9737316
Pseudo is Norm-conserving + core correction, Zval = 23.0
Generated using ONCVPSP code by D. R. Hamann
Using radial grid of 1358 points, 6 beta functions with:
l(1) = 0
l(2) = 0
l(3) = 1
l(4) = 1
l(5) = 2
l(6) = 2

atomic species  valence    mass      pseudopotential
Ta            27.00  180.94790    Ta( 1.00)
As            23.00  74.92160    As( 1.00)

```

Fig 3.15: PPs details in the QE output file

```

site n.      atom          positions (alat units)
 1           Ta  tau( 1) = ( 0.000000  0.000000  2.5558870 )
 2           Ta  tau( 2) = ( 0.000000  0.4999994  3.4078862 )
 3           Ta  tau( 3) = ( 0.4999994  0.4999994  0.8518880 )
 4           Ta  tau( 4) = ( 0.4999994  0.000000  1.7038875 )
 5           As  tau( 5) = ( 0.000000  0.000000  1.1336096 )
 6           As  tau( 6) = ( 0.000000  0.4999994  1.9856088 )
 7           As  tau( 7) = ( 0.4999994  0.4999994  2.8376083 )
 8           As  tau( 8) = ( 0.4999994  0.000000  0.2816101 )

number of k points=    4 Gaussian smearing, width (Ry)=  0.0100
                      cart. coord. in units 2pi/alat
k( 1) = ( 0.000000  0.000000  0.000000), wk =  0.1111111
k( 2) = ( 0.000000  0.3333333  0.000000), wk =  0.2222222
k( 3) = ( 0.3333333  0.3333333  0.000000), wk =  0.4444444
k( 4) = ( 0.3333333  0.000000  0.000000), wk =  0.2222222

Dense grid: 53493 G-vectors FFT dimensions: ( 32, 32, 108)
Smooth grid: 15907 G-vectors FFT dimensions: ( 24, 24, 72)

Estimated max dynamical RAM per process > 113.74 MB

Check: negative core charge= -0.001495
Generating pointlists ...
new r_m : 0.3129 (alat units) 2.0359 (a.u.) for type 1
new r_m : 0.3129 (alat units) 2.0359 (a.u.) for type 2

Initial potential from superposition of free atoms

starting charge 199.99538, renormalised to 200.00000
Starting wfcs are 120 randomized atomic wfcs

total cpu time spent up to now is 2.9 secs

```

Fig 3.16: The coordinates and the k-points of the system along with the memory requirement for the calculation details in the QE output file

```

Self-consistent Calculation

iteration # 1      ecut= 25.00 Ry      beta= 0.40
Davidson diagonalization with overlap
ethr = 1.00E-02, avg # of iterations = 6.5

total cpu time spent up to now is 18.9 secs

total energy          = -4471.07144289 Ry
estimated scf accuracy < 487.97483813 Ry

total magnetization   = 1.73 Bohr mag/cell
absolute magnetization = 1.83 Bohr mag/cell

```

Fig 3.17: The scf calculation details in the QE output file.

```

iteration # 23      ecut= 25.00 Ry      beta= 0.40
Davidson diagonalization with overlap
ethr = 1.72E-09, avg # of iterations = 5.8

total cpu time spent up to now is 243.6 secs

End of self-consistent calculation

```

Fig 3.18: The end of scf calculation details in the QE output file.

```

k = 0.3333 0.0000 0.0000 ( 1976 PWs) bands (ev):
-256.5953-256.1831-256.1220-255.7708-132.0140-131.0559-130.2848-129.8648
-129.6140-129.3247-129.3003-128.2130-128.2107-128.2028-128.1958-127.9236
-127.8834-127.7263-127.1744-126.9662 -69.2339 -69.1788 -69.1720 -69.1469
-69.1325 -69.1181 -69.0802 -69.0758 -69.0603 -69.0532 -69.0342 -69.0309
-5.4958 -4.9630 -4.9363 -4.7965 -4.7146 -4.6074 -4.6022 -4.5635
-4.5357 -4.4998 -4.4784 -4.4507 -4.4449 -4.4104 -4.3946 -4.3910
-4.3576 -4.3304 -4.3230 -4.3083 -4.1765 -4.1107 -3.9822 -3.9678
-3.9135 -3.8719 -3.4716 -3.3223 -3.0888 -3.0381 -2.7010 -2.2544
-2.2278 -2.2204 -2.2178 -2.1980 -2.0430 -1.8431 -1.3739 -0.7252
4.3003 4.7548 4.8819 5.2263 12.2491 12.6159 13.0375 13.7015
19.0932 21.3244 21.6163 22.7152 22.8855 23.9872 24.2276 24.8462
25.5527 26.1671 26.5085 26.5111 27.4168 27.5501 28.1640 28.2516
28.4743 28.5300 28.6025 28.8431 28.8981 28.9761 28.9834 29.1623
29.1699 29.2803 29.3884 29.8673 29.9272 29.9586 29.9960 30.2350
30.2837 30.6738 30.8705 31.0648 31.1411 31.3734 31.4487 31.7776

the Fermi energy is 28.4993 ev

! total energy = -4513.88434915 Ry
estimated scf accuracy < 0.00000095 Ry
smearing contrib. (-TS) = -0.00984387 Ry
internal energy E=F+TS = -4513.87450529 Ry

The total energy is F=E-TS. E is the sum of the following terms:
one-electron contribution = -2037.33259895 Ry
hartree contribution = 978.60177519 Ry
xc contribution = -546.93655314 Ry
ewald contribution = -2908.20712838 Ry

total magnetization = 3.11 Bohr mag/cell
absolute magnetization = 3.16 Bohr mag/cell

convergence has been achieved in 23 iterations

```

Fig 3.19: The details about the calculated energy, k points, fermi energy and magnetization is provided at the last.

The contents in the output file differs according to the input provided. It depends on the system and what properties are calculated.

### 3.9. Structural optimization using QE and VESTA

Geometry optimization or structure optimization using DFT is done by moving the atoms of a molecule to get the most stable structure with the lowest possible ground state energy. There are two types of structural optimization calculations in QE:

- relax: where only the atomic positions are allowed to vary, and
- vc-relax: which allows to vary both the atomic positions and lattice constants.

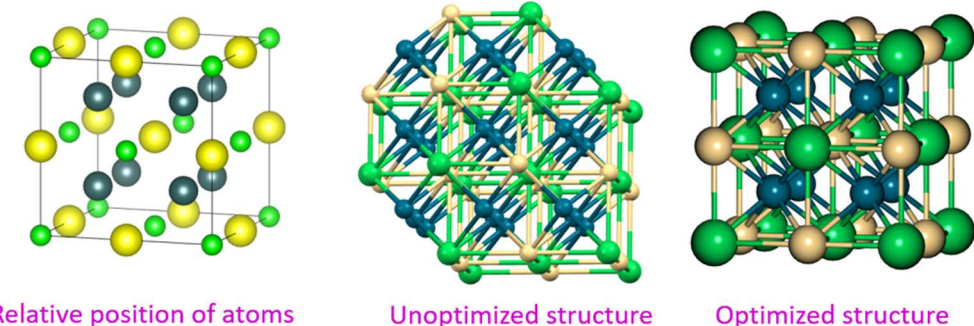


Fig 3.20: structural optimization of TmCdPd<sub>2</sub> (Heusler)

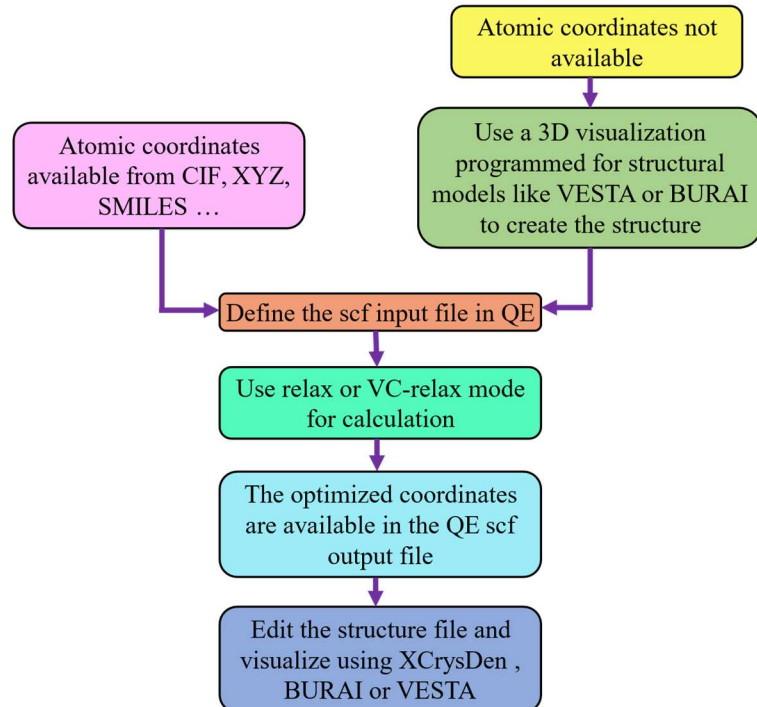


Fig 3.21: Flow chart representing the procedure structural optimization of a system

### 3.10. Calculation for DOS, PDOS and Band structure

To run a DOS calculation

1. Perform a scf `pw.x` calculation (`calculation='scf'`)
2. Perform a non-scf `pw.x` calculation (`calculation='nscf'`)
  - i. use a denser k-point mesh
  - ii. use `occupations='tetrahedra'` in &SYSTEM card
  - iii. Use `nosym = .TRUE.`
3. Perform a `dos.x` calculation
4. Perform a `projwfc.x` calculation to obtain PDOS projected to atomic states.

To run a BAND calculation

1. Perform a scf `pw.x` calculation (`calculation='scf'`)
2. Perform a bands type non-scf calculation using `pw.x` calculation (`calculation='bands-nscf'`)
  - i. use a denser k-point mesh and suitable k-paths.
  - ii. use `occupations='tetrahedra'` in &SYSTEM card
  - iii. Use `nosym = .TRUE.`
3. Perform a `bands.x` calculation  
`bands.x <input.in> output.out`

The following changes are made in the scf input file to run the bands calculation

```
&control
  calculation = 'bands'
  prefix = 'TaAs'
  pseudo_dir = '/path/to/pseudopotentials/'
  outdir = './'
/
.
.

K_POINTS {tpiba_b}          //The high symmetry k-points
10
0.0      0.0      0.0      1.0
0.1      0.0      0.0      1.0
...
0.5      0.5      0.5      1.0
/
&BANDS
lsym      = .FALSE.
spin_component = 1
/

```

### 3.10.1. Selecting the High symmetry K-points

Selecting high-symmetry k-points is essential for band structure calculations as it allows you to efficiently sample the Brillouin zone and visualize the electronic structure of your material along important symmetry directions.

- Identify the Brillouin Zone (BZ) of the Crystal: Understand the symmetry of the crystal structure. This typically involves knowing the lattice parameters and the space group of the crystal.
- Refer to Symmetry Tables: Use symmetry tables or databases specific to the crystal structure to identify the high-symmetry points and lines in the Brillouin zone. These tables are often available in textbooks on solid-state physics or online resources related to crystallography.
- Consult Brillouin Zone Diagrams: Look at Brillouin zone diagrams relevant to the crystal system. These diagrams depict the high-symmetry points and lines in the Brillouin zone.
- Select High-Symmetry Points: Choose a set of high-symmetry k-points that span the important symmetry directions in the Brillouin zone. Commonly used high-symmetry points include the  $\Gamma$  point (centre of the Brillouin zone), X, Y, Z, R, M, A, and L points, depending on the crystal symmetry.

- Define Path in Reciprocal Space: Once the high-symmetry points are selected, define a path in reciprocal space that connects these points. This path should pass through important symmetry lines and planes in the Brillouin zone.
- Generate K-Point Path: Use software tools or scripts to generate a list of k-points that define the path in reciprocal space. These k-points will be used as input for your band structure calculation.

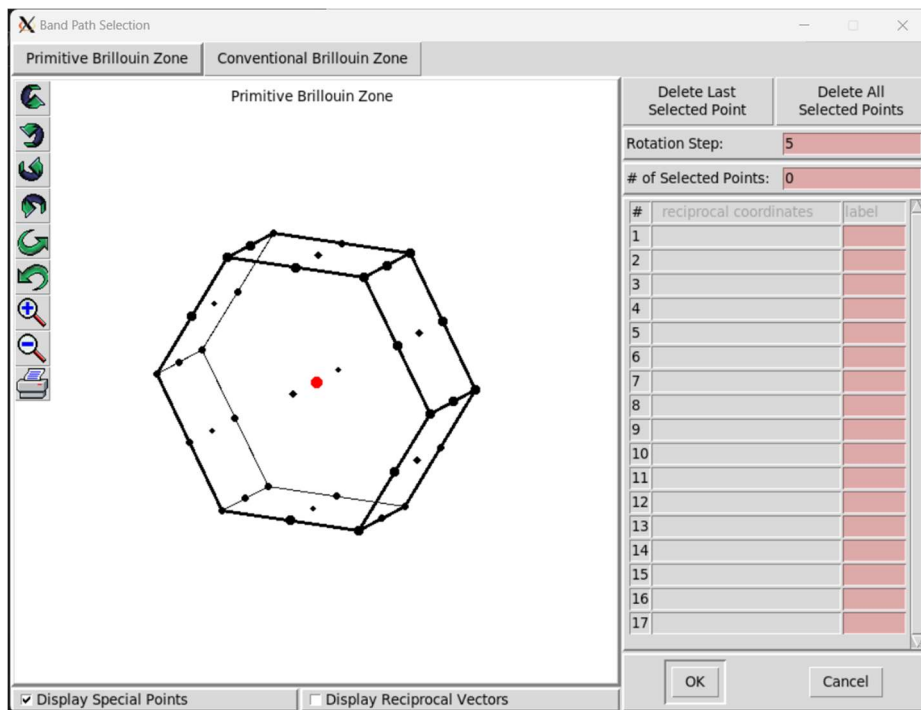


Fig 3.22: The K-point selection tool in XCrysDen. The BZ of MoS<sub>2</sub> is represented here.

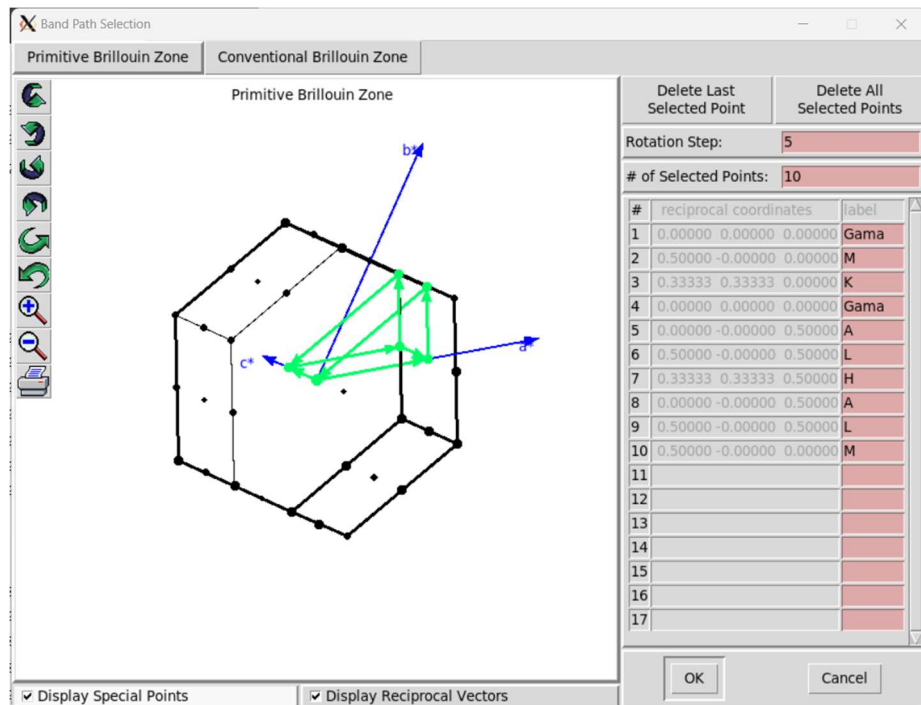


Fig 3.23: The high symmetry k-points in scaled units of MoS<sub>2</sub>. The high symmetric k-path ( $\Gamma$ —M—K— $\Gamma$ —A—L—H—A|L—M) is represented in green vectors in the reciprocal space.

### 3.11. Calculation of Absorption spectra

The `turbo_lanczos.x` program allows us to calculate absorption spectra of molecules using time-dependent density functional perturbation theory (TDDFPT) without computing empty states. The interactions of electrons (Hartree and Exchange-Correlation effects) are considered fully in ab initio and self-consistently. The electronic transitions from occupied to empty states cannot be analysed (use `turbo_davidson.x` for this purpose). The overall absorption spectrum in a wide frequency range can be calculated at once [27] [28] [29].

- Perform a SCF ground-state calculation

```
pw.x <input.in> output.out
```

- Perform Lanczos recursions using `turbo_lanczos.x` program

```
turbo_lanczos.x < Benzene.lanczos.in > Benzene.lanczos.out
```

- Perform a spectrum calculation using post-processing program `turbo_spectrum.x` and using the Lanczos coefficients computed in the previous step get the data points to plot the absorption data.

```
turbo_spectrum.x < Benzene.tddfpt_pp.in > Benzene.tddfpt_pp.out
```

```
&LR_INPUT
prefix = 'MNA'
outdir = './outdir'
restart_step = 100,
restart = .false
/
&LR_CONTROL
itermax = 10000
ipol = 3
/
```

Fig 3.24: `turbo_lanczos.x` input file for MNA

```
Lanczos iteration:      3  Pol:1
lr_apply_liouvillian: not applying interaction
alpha(00000003)=  0.000000
beta (00000003)= 12.163815
gamma(00000003)= 12.163815
z1=          1  0.00000000000000E+00  0.00000000000000E+00
z1=          2  0.00000000000000E+00  0.00000000000000E+00
z1=          3  0.00000000000000E+00  0.00000000000000E+00
```

Fig 3.25: `turbo_lanczos.x` out file for MNA

```
&LR_INPUT
prefix = 'MNA'
outdir = './outdir'
itermax0 = 10000
itermax = 20000
extrapolation = 'osc'
start = 0.0
end = 50.0
increment = 0.01
epsil = 0.01
ipol = 4
/
```

Fig 3.26: `turbo_spectrum.x` input file for MNA

```

\hbar \omega(eV) Re(chi) (e^2*a_0^2/eV) Im(chi) (e^2*a_0^2/eV)
chi_1_1= 0.00000000000000E+00 0.367809385681014E+02 -.00000000000000E+00
chi_2_1= 0.00000000000000E+00 -.631858329281267E-04 0.00000000000000E+00
chi_3_1= 0.00000000000000E+00 -.204467248171178E+02 0.00000000000000E+00
chi_1_2= 0.00000000000000E+00 -.631706192483719E-04 0.00000000000000E+00
chi_2_2= 0.00000000000000E+00 0.250012382752616E+02 -.00000000000000E+00
chi_3_2= 0.00000000000000E+00 0.358096420342268E-04 -.00000000000000E+00
chi_1_3= 0.00000000000000E+00 -.204463946327822E+02 0.00000000000000E+00
chi_2_3= 0.00000000000000E+00 0.358450506838120E-04 -.00000000000000E+00
chi_3_3= 0.00000000000000E+00 0.205248428246752E+02 -.00000000000000E+00
chi_1_1= 0.10000000000000E-01 0.367810680070323E+02 0.207145008754846E-01
chi_2_1= 0.10000000000000E-01 -.631868517748287E-04 -.187715955097414E-06
chi_3_1= 0.10000000000000E-01 -.204467950141741E+02 -.112857575489507E-01
chi_1_2= 0.10000000000000E-01 -.631716378970102E-04 -.187509351059613E-06
chi_2_2= 0.10000000000000E-01 0.250012789479554E+02 0.607690777777168E-02
chi_3_2= 0.10000000000000E-01 0.358101583277243E-04 0.954462827239609E-07

```

Fig 3.27: turbo\_spectrum.x output file for MNA

Directly running the program in the terminal will reduce the errors in the inputs for calculation as namelist errors frequently occur in the QE input files.

### 3.12. System parameters

All the calculation were done using Personal computer with the following specifications

- Processor - 11th Gen Intel(R) Core(TM) i5-1135G7
- RAM – 16GB (SSD)
- Operating system – UBUNTU (Linux), Windows 11
- Cores – 4
- GPU – 2GB

Most of the calculations are run parallelly utilizing the 4 available cores. The average time for scf calculations is 10 to 30 min. The average time for DOS calculations is 1hr, the average time for the bands calculations is 5 to 10 hr, the average time for the absorption spectra is 5 to 10 hr. This is the minimum configuration for running any DFT code.

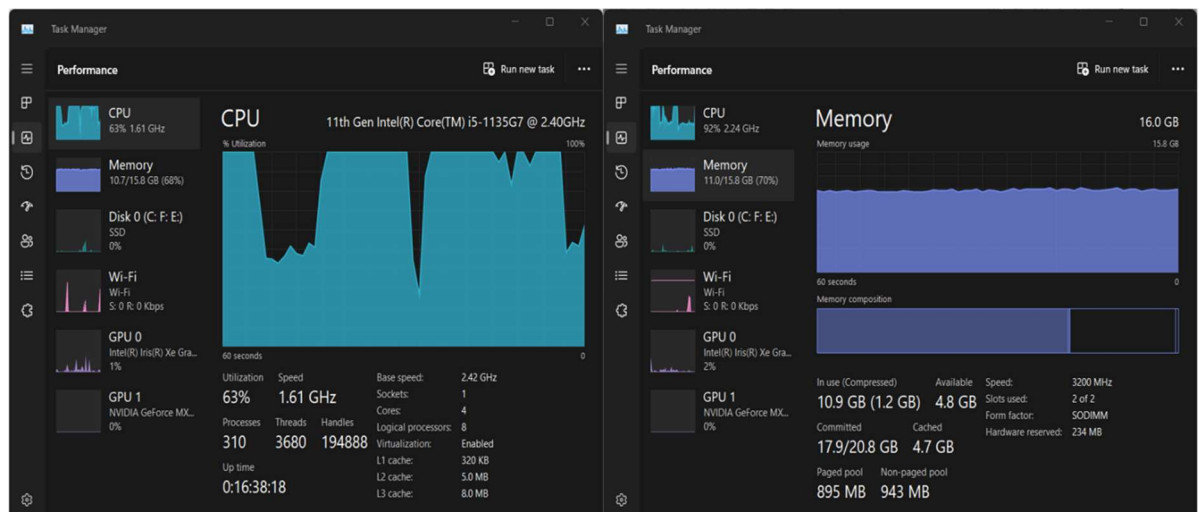


Fig 3.28: CPU and Memory utilization while running the code.

### 3.13. Other tools used

Other than the QE package other tool is used for various purpose. Mainly to visualize and modify the structure and for post processing the results obtained from the QE calculations. A short description of tools used is discussed below.

#### 3.13.1. VESTA

VESTA is a widely-used software package for visualizing and analysing crystal structures. It is particularly popular among researchers in materials science, chemistry, and solid-state physics. It is available in Windows, Linux and Mac OS system. The following operations can be done using VESTA [30].

- Visualization of molecular and crystal structure.
- **Crystal Structure Editing:** VESTA enables users to create, modify, and manipulate crystal structures. Users can add atoms, change their positions, and adjust lattice parameters. This feature is useful for constructing new crystal structures or refining existing ones.
- **Property Visualization:** VESTA allows users to visualize various properties associated with crystal structures, such as electron density, electrostatic potential, and magnetic moments.
- **Symmetry Analysis:** VESTA includes tools for analysing the symmetry of crystal structures. Users can identify symmetry elements, generate symmetry-related positions, and visualize symmetry operations.
- **File Format Support:** VESTA supports a wide range of file formats commonly used to represent crystal structures, including CIF (Crystallographic Information File), VASP POSCAR/CONTCAR, XYZ, and more.
- **Integration with Computational Tools:** VESTA can be integrated with various computational tools and software packages used in materials science and chemistry. For example, it can interface with density functional theory (DFT) codes for structural optimization and property calculations.
- Generation of simulated powdered XRD pattern.

#### 3.13.2. XCrySDen

XCrySDen (X-Window Crystal Structure Display Engine) is a powerful software package designed for visualizing and analysing crystal structures. It efficiently runs in the Linux environment, considerably it is slow but has a huge set of functionalities for analysing crystal structures. The features of XCrySDen are mentioned below [31].

- **3D Visualization:** XCrySDen provides a highly interactive 3D visualization environment for crystal structures
- **Density Visualization:** XCrySDen allows users to visualize various density-related properties, such as electron density and charge density.
- **Property Visualization:** Users can visualize a wide range of properties associated with crystal structures, including magnetic moments, vibrational modes, and electron localization functions.
- Integration with the QE package and other DFT codes like ELK code.

### 3.13.3. Python

Python's pyscf library is commonly used to compute density functional theory (DFT). AS it is integrated with SIESTA the convergence of the system can be tested with the QE package. Other than the graph and crystal positions can be calculated and visualized using python. Here mainly python is mainly used as a visualization tool. It is used for pre-processing and post processing toll and to automate the process.

The "cell to CIF" informal package is a set of tools and utilities designed to facilitate the conversion of crystal structure data from various formats into the Crystallographic Information File (CIF) format. The package supports input data in various formats commonly used to represent crystal structures, such as XYZ, POSCAR/CONTCAR, CIF, etc. This versatility allows users to convert crystal structure data from different sources and software packages into CIF format [32].

### 3.13.4. BURAI

BURAI is a graphical user interface (GUI) software designed to facilitate the use of QE code in windows. BURAI serves as a front-end interface for popular quantum chemistry software packages such as Quantum ESPRESSO, VASP, and Gaussian. URAI simplifies the process of setting up input files for electronic structure calculations. Users can specify parameters, define input structures, and select appropriate methods and basis sets through intuitive graphical interfaces. This helps streamline the preparation of input files, reducing the likelihood of errors and ensuring consistency. The software provides visualization capabilities for analysing the results of electronic structure calculations [33].

### **3.13.5. Origin**

Origin is a powerful software package primarily used for data analysis and visualization. It provides a wide range of tools for analysing, graphing, and interpreting data. Origin allows users to import data from various sources, including Excel files, ASCII files, and databases. Users can easily manipulate data sets, perform data transformations, filter data, and handle missing values. One of the main features of Origin is its robust graphing capabilities. Users can create a wide variety of 2D and 3D plots, including scatter plots, line graphs, bar charts, histograms, contour plots, and surface plots [34].

### **3.13.6. Fortran**

The heart of Quantum ESPRESSO consists of computational kernels written in Fortran. These kernels perform key tasks such as solving the Kohn-Sham equations, evaluating electronic densities, computing forces on atoms, and optimizing atomic positions. Fortran's efficiency in numerical computation makes it well-suited for implementing these computational algorithms. Quantum ESPRESSO interfaces with external numerical libraries written in Fortran, such as LAPACK (Linear Algebra Package) and FFT (Fast Fourier Transform) libraries. These libraries provide efficient implementations of matrix operations, eigen solvers, and Fourier transforms, enhancing the performance and capabilities of Quantum ESPRESSO. Quantum ESPRESSO interfaces with external numerical libraries written in Fortran, such as LAPACK (Linear Algebra Package) and FFT (Fast Fourier Transform) libraries. These libraries provide efficient implementations of matrix operations, eigen solvers, and Fourier transforms, enhancing the performance and capabilities of Quantum ESPRESSO.

### **3.13.7. FFT and LAPACK**

LAPACK, which stands for Linear Algebra Package, is a widely-used software library for numerical linear algebra computations. It provides efficient and reliable implementations of routines for solving systems of linear equations, least squares problems, eigenvalue problems, singular value decomposition (SVD), and other matrix-related operations.

FFT, or Fast Fourier Transform, is an algorithm used to compute the Discrete Fourier Transform (DFT) and its inverse. It efficiently transforms a time-domain signal into its frequency-domain representation and vice versa, enabling the analysis and manipulation of signals and data in the frequency domain.

## CHAPTER 4

### First-principles calculations of urea and 2-methyl-4-nitroaniline

#### 4.1. Organic crystals

Organic crystals refer to crystalline structures composed of organic molecules. These molecules are primarily made up of carbon atoms bonded to hydrogen, along with other elements such as oxygen, nitrogen, sulphur, and halogens. Organic crystals pose significant challenges for computational methods due to several factors:

- Complexity of Molecular Structure: Organic molecules can have intricate structures with numerous atoms and functional groups. Modelling the behaviour of these molecules within a crystal lattice requires accurate representation of their geometry and intermolecular interactions.
- Intermolecular Interactions: the interplay between different strengths of bonding types in molecular crystals (i.e., the strong intra-molecular covalent bonds vs much weaker inter-molecular Van der Waals and possibly hydrogen bonds).
- Large Unit Cells: Organic crystals can have large unit cells containing many molecules. This increases the computational cost of simulating these systems, as more atoms need to be included in the calculations.
- Flexibility and Dynamics: Organic molecules can exhibit flexibility and dynamic behaviour, such as conformational changes and molecular rotations. Capturing these dynamics accurately in computational models is challenging and requires methods that can handle molecular motion and flexibility.
- Polymorphism and Solvates: Organic crystals often exist in multiple polymorphic forms or as solvates with solvent molecules incorporated into the crystal structure. Predicting the preferred crystal form or understanding the impact of solvent molecules on crystal properties requires advanced computational techniques.

In this work the Urea and 2-methyl-4-nitroaniline (MNA) molecules are chosen and their electronic properties has been calculated using the QE code. There has been reported literature for UREA but for MNA only few literatures available in this field of DFT calculations [1].

## 4.2. Urea

Urea, chemically known as  $CO(NH_2)_2$ , is an organic compound widely recognized for its importance in various industrial and biological applications. Its crystalline form, urea crystals, has garnered significant attention due to its unique properties and diverse applications. Urea is also called carbamide because it is a diamide of carbonic acid,. This amide has two amino groups ( $-NH_2$ ) joined by a carbonyl functional group ( $-C(=O)-$ ). It is thus the simplest amide of carbamic acid [35].

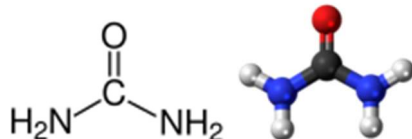


Fig 4.1: Chemical symbol and molecular diagram of Urea molecule.

### 4.2.1. Crytal structure of Urea

The bulk urea crystal is taken for calculation which consist of 64 atoms. This structure has 194 electrons which contribute to the electronic charge density of the molecule with 192 KS states.

Urea Crystallizes in the tetragonal  $\bar{P}42_1m$  space group. The structure is zero-dimensional and consists of two  $CO(NH_2)_2$  clusters.  $C^{4+}$  is bonded in a trigonal planar geometry to two equivalent  $N^{3-}$  and one  $O^{2-}$  atom. Both C-N bond lengths are 1.34 Å. The C-O bond length is 1.27 Å.  $N^{3-}$  is bonded in a trigonal planar geometry to one  $C^{4+}$  and two  $H^{1+}$  atoms. Both N-H bond lengths are 1.01 Å. There are two inequivalent  $H^{1+}$  sites. In the first  $H^{1+}$  site,  $H^{1+}$  is bonded in a single-bond geometry to one  $N^{3-}$  atom. In the second  $H^{1+}$  site,  $H^{1+}$  is bonded in a single-bond geometry to one  $N^{3-}$  atom.  $O^{2-}$  is bonded in a single-bond geometry to one  $C^{4+}$  atom [2].

The lattice parameters were fully optimized and the atomic positions are also relaxed and found the lattice parameters as  $a = 5.561000 \text{ \AA}$ ,  $b = 5.561000 \text{ \AA}$ ,  $c = 4.71200 \text{ \AA}$  and  $\alpha = \beta = \gamma = 90^\circ$ . Urea follows a primitive tetragonal crystal system having a point group  $42m$  and space group  $P42_1m$ . And the unit cell ahs a volume of  $151.005076 \text{ \AA}^3$ .

The urea molecule is planar when in a solid crystal because of  $sp^2$  hybridization of the n orbitals. The urea molecule is planar when in a solid crystal because of  $sp^2$  hybridization of the n orbitals. The crystal structure of urea is stabilized by intermolecular hydrogen bonds formed between urea molecules. Each urea molecule can form four hydrogen bonds: two

through its amine ( $\text{NH}_2$ ) groups and two through its carbonyl ( $\text{C=O}$ ) group. This extensive hydrogen bonding network leads to the formation of layers of urea molecules within the crystal lattice. Within these layers, urea molecules are arranged in a zigzag pattern, with each molecule forming hydrogen bonds with its neighbouring molecules. The hydrogen bonds between urea molecules contribute to the stability of the crystal structure and influence its physical properties, such as solubility and melting point. Overall, the crystal structure of urea is characterized by its layered arrangement of molecules held together by hydrogen bonding interactions.

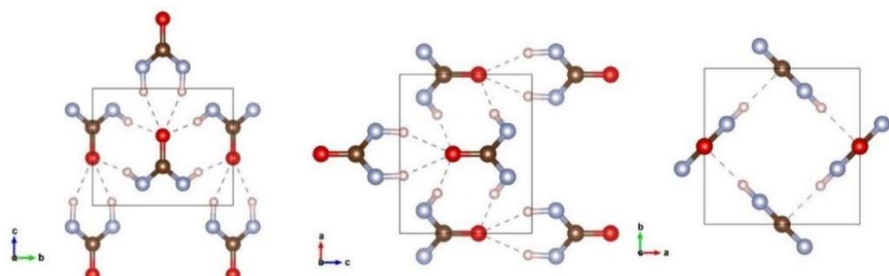


Fig 4.2: The urea crystal in different orientations

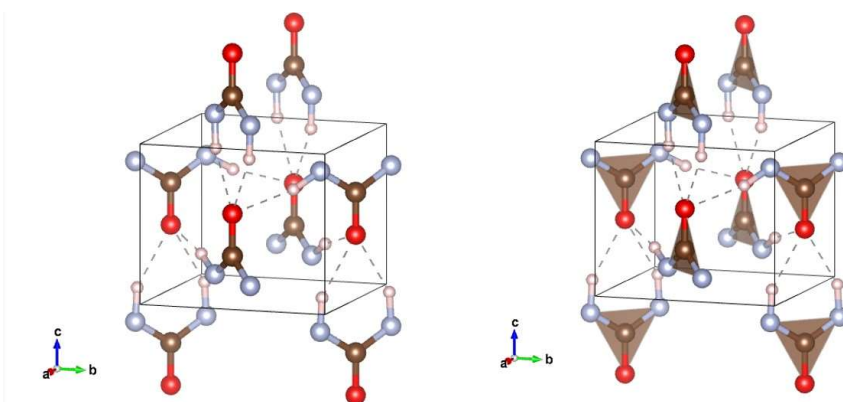


Fig 4.3: The bulk urea crystal for which the calculations are performed.

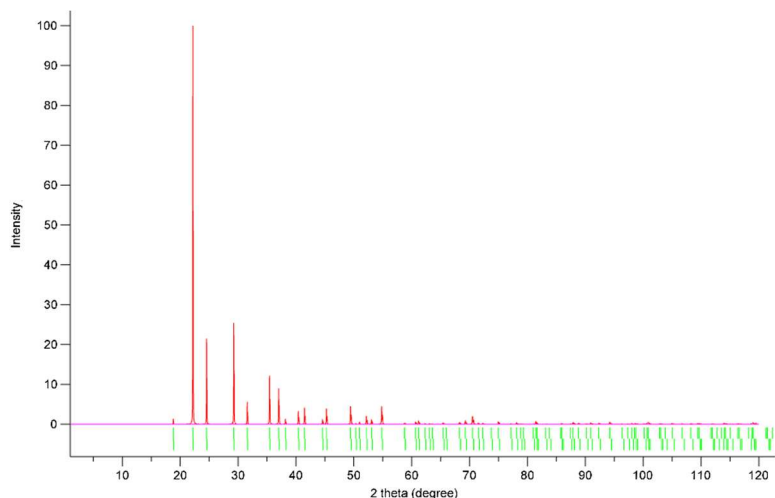


Fig 4.4: Simulated XRD of urea

The convergence for the Urea structure has been achieved in 8 iterations with total energy  $-702.47 \text{ Ry}$ .

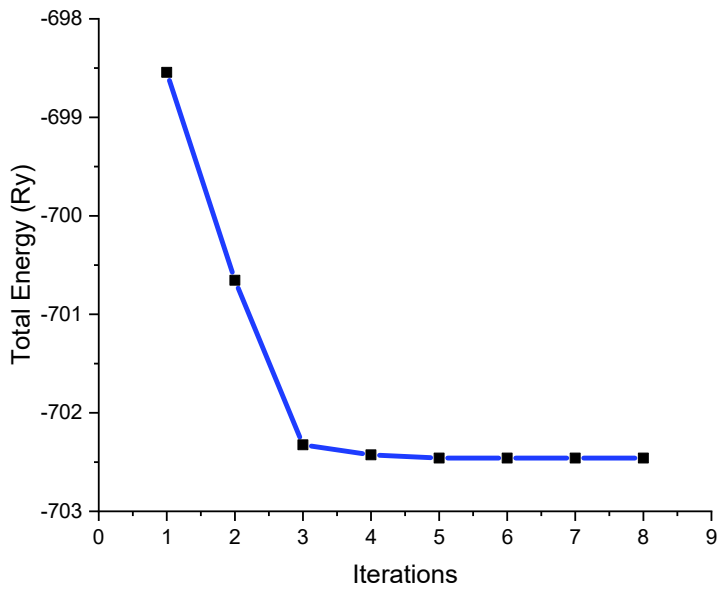


Fig 4.5: Convergence of total energy with respect to total energy of Urea.

#### 4.2.2. Electronic property of urea

The electronic structure calculation was performed using QE code with the following input parameters. The BZ sampling was done using the k-point grid of  $3 \times 3 \times 9$  according the Monkhorst -pack scheme. The convergence limit is chosen to be  $1 \times 10^{-6} \text{ Ry}$  with the PW kinetic energy cut-off of  $25 \text{ Ry}$  and charge density cutoff of  $225 \text{ Ry}$ . The calculations were performed using the relax structure of Urea in its ground state. The energy bands are calculated along the high symmetric k-path.

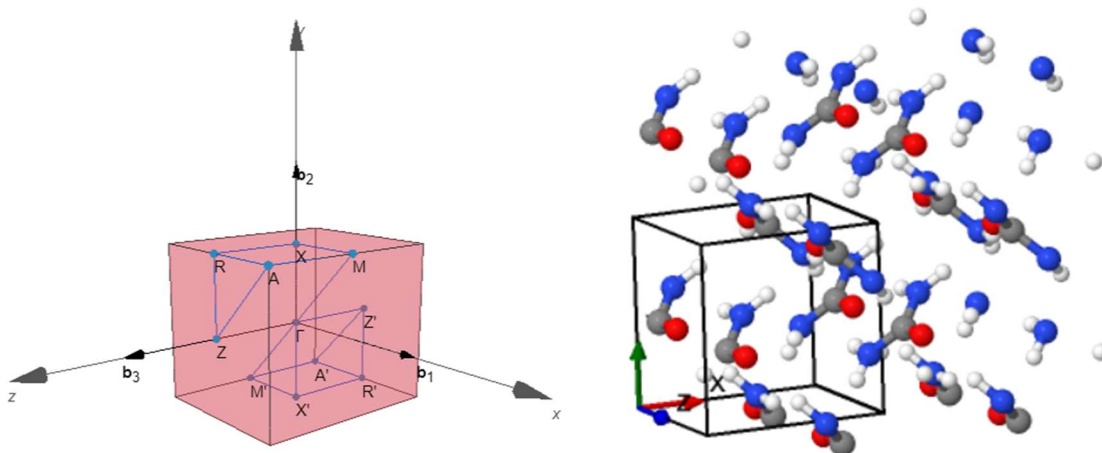


Fig 4.6.: The high symmetric K-points and the unit cell of the bulk urea in relaxed structure

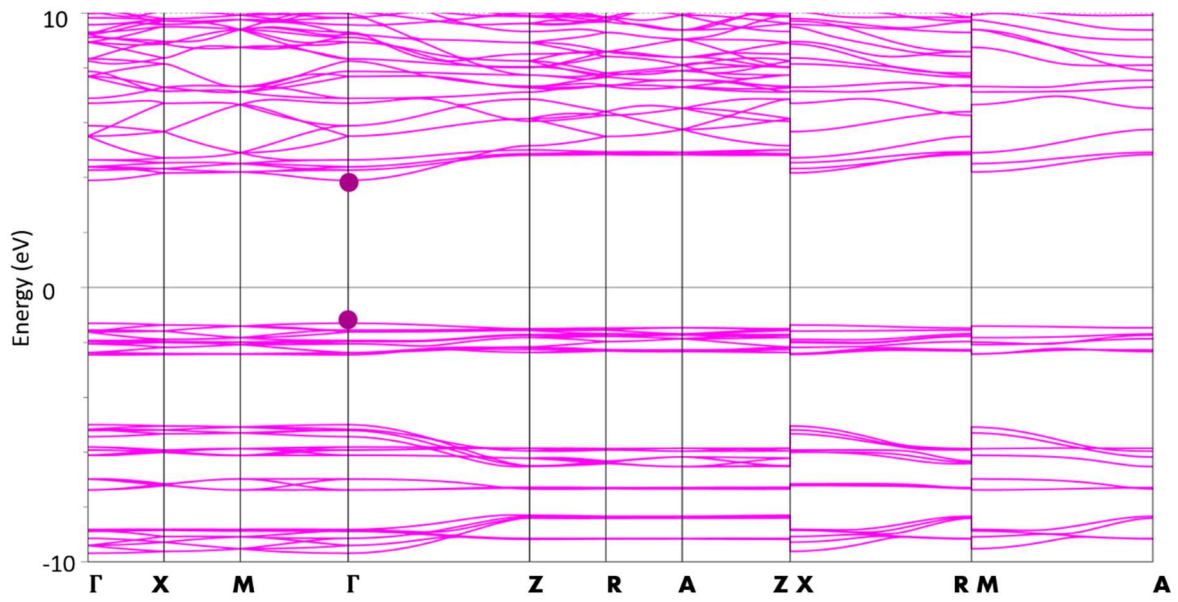


Fig 4.7: Band electronic band structure of Urea

The electronic band structure is plotted by keeping the fermi energy as the reference. The fermi energy calculated is 1.502 eV. Urea in its crystal form has a direct band gap of  $\sim 5.4$  eV which agrees with the results available. The band structure reveals that Urea is an insulator.

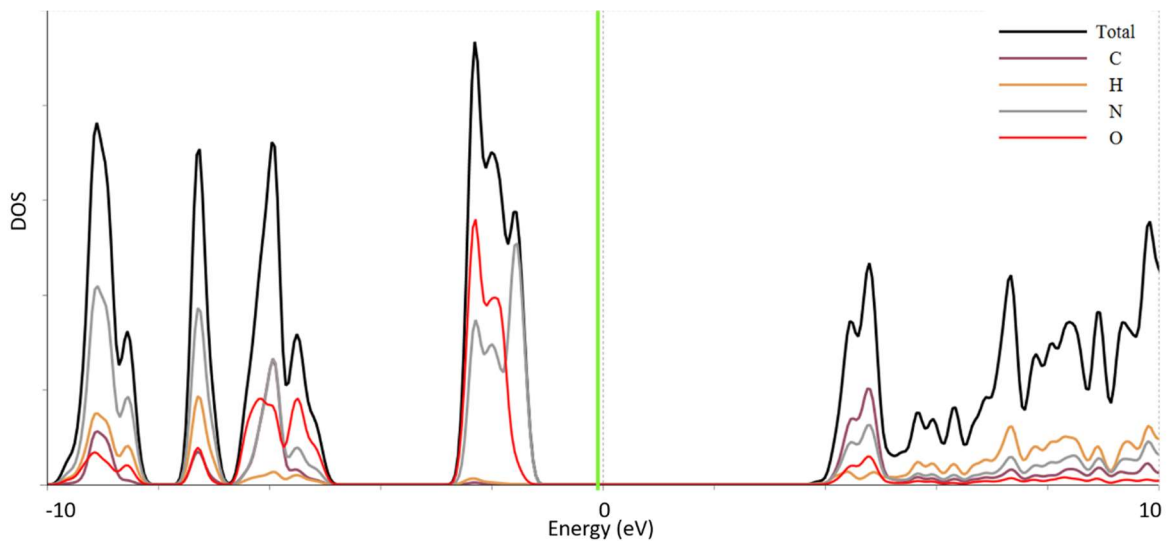


Fig 4.8: The Density of states (DOS) of urea with fermi energy kept as reference.

From the DOS plot it is seen that the Oxygen and Nitrogen have the maximum contribution of electrons in both valence band and conduction band. In the conduction band the contribution of carbon is relatively high.

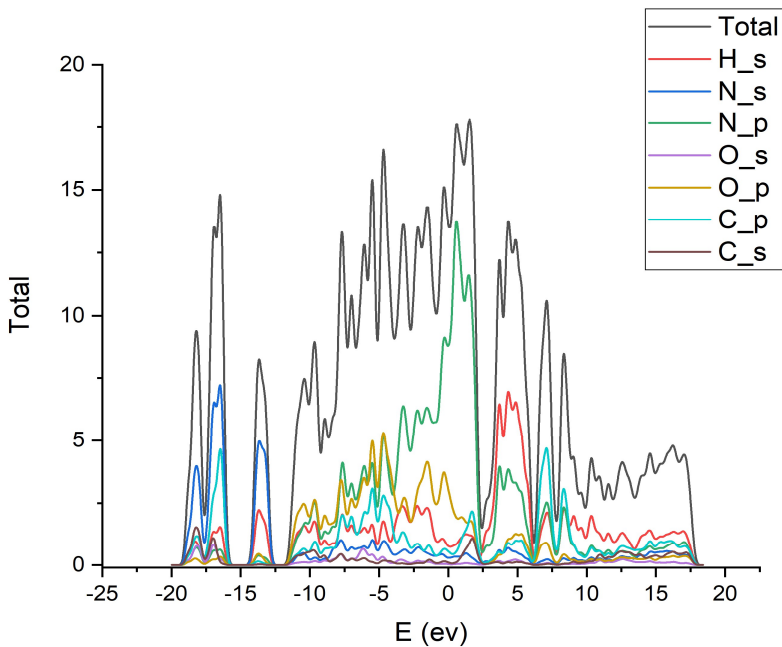


Fig 4.9: Projected density of states (PDOS) of urea

From the PDOS it is found that the p orbital of nitrogen has the maximum contribution in the bonding. The hydrogen bonding in urea is evident by its contribution in the bonding. Thus, the PDOS gives a overall view of the bonding involved in the Urea molecule.

The total energy of the molecule in its ground state is  $-713.21\text{ Ry}$  and the lowest occupied level is found to be  $0.2421\text{ eV}$  and the highest occupied level is found to be  $0.6824\text{ eV}$ .

### 4.3. 2-methyl-4-nitroaniline (MNA)

2-methyl-4-nitroaniline (MNA) is an organic compound with the chemical formula  $C_7H_8N_2O_2$ . It is also known by other names such as 4-nitro-2-methylaniline or N-methyl-p-nitroaniline. The molecule consists of an aniline group, which is a benzene ring with an amino group attached, and it has two substituent groups: a methyl group attached at the 2-position and a nitro group attached at the 4-position. MNA is typically a yellow solid at room temperature [36].

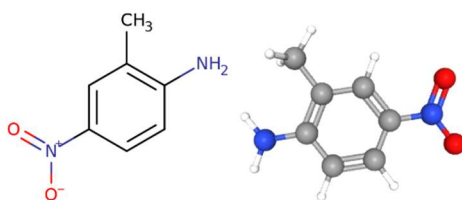


Fig 4.10: Chemical symbol and molecular diagram of MNA

### 4.3.1. Crystal structure

2-methyl-4-nitroaniline crystallizes in the monoclinic system, space group  $Cc$  (Unique axis b) with four molecules in the unit cell. The lattice parameters were fully optimized and the atomic positions are also relaxed and found the lattice parameters as  $a = 10.72 \text{ \AA}$ ,  $b = 11.57 \text{ \AA}$ ,  $c = 7.46 \text{ \AA}$  and  $\alpha = \gamma = 90^\circ$ ,  $\beta = 130.42^\circ$ . With the unit cell volume of  $705.74 \text{ \AA}^3$ . The system contains 76 atoms in total.

The calculated C–H bonds are slightly longer than their experimental counterparts. Due to the electron withdrawing effects of the nitro group, those C–C bonds which are along the long molecular axis are shorter than other C–C bonds. In addition, the C–C bonds which are near the amino group are longer than those which are near the nitro-group. Such differences show that the benzene ring which acts as a molecular bridge plays a major role in electron delocalization. Due to the near dipolar structure, those bond lengths which are located in the meta position (are longer than those located in the para-position [36].

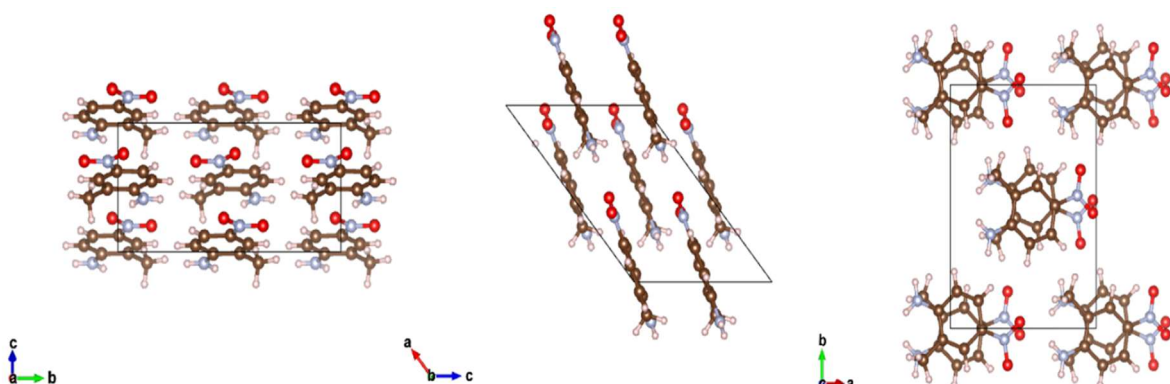


Fig 4.11: The MNA crystal in different orientations in the real space

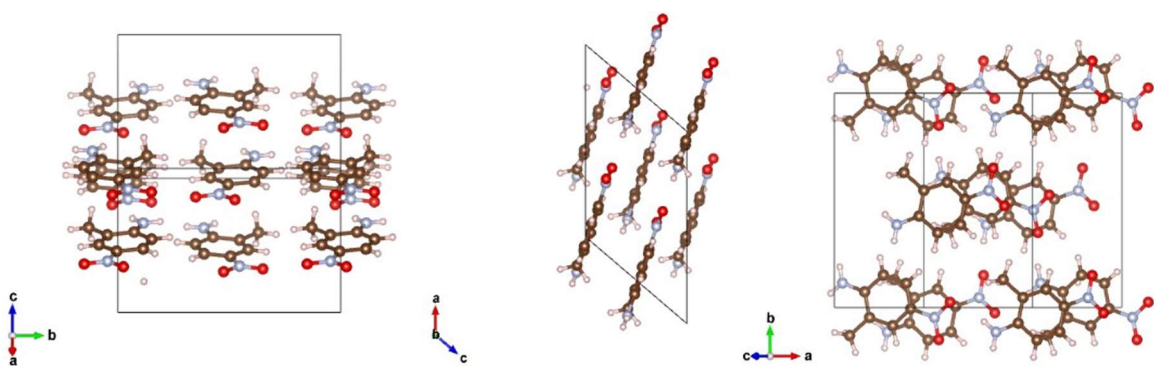


Fig 4.12: The MNA crystal in different orientations in the reciprocal space

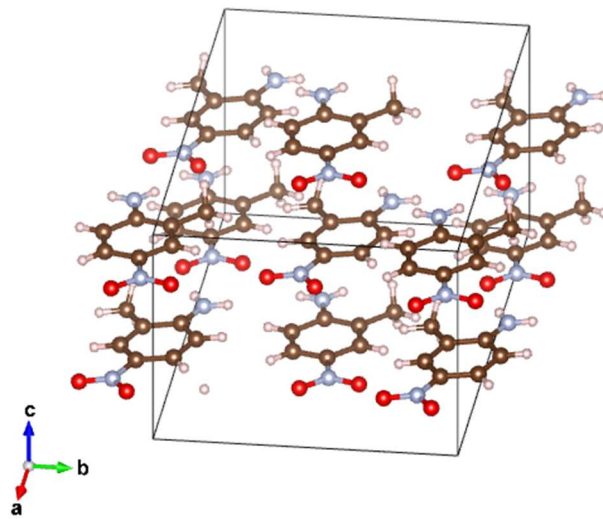


Fig 4.13: The bulk MNA crystal for which the calculations are performed.

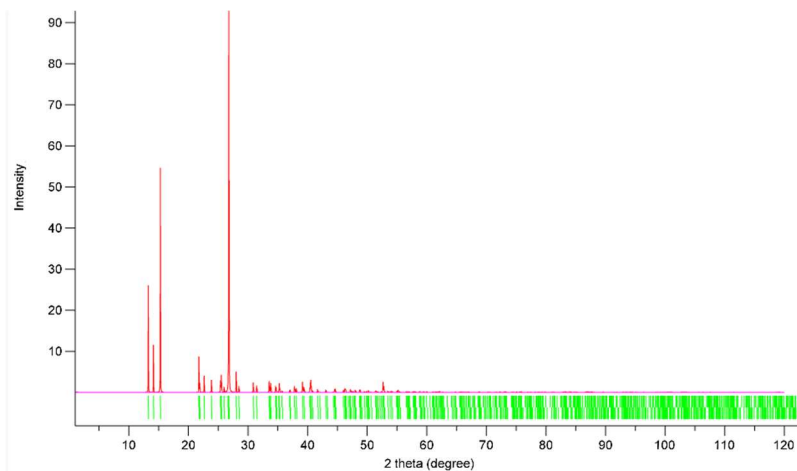


Fig 4.14: Simulated XRD of MNA

The convergence for the Urea structure has been achieved in 8 iterations with total energy  
 $-768.80528942 \text{ Ry}$

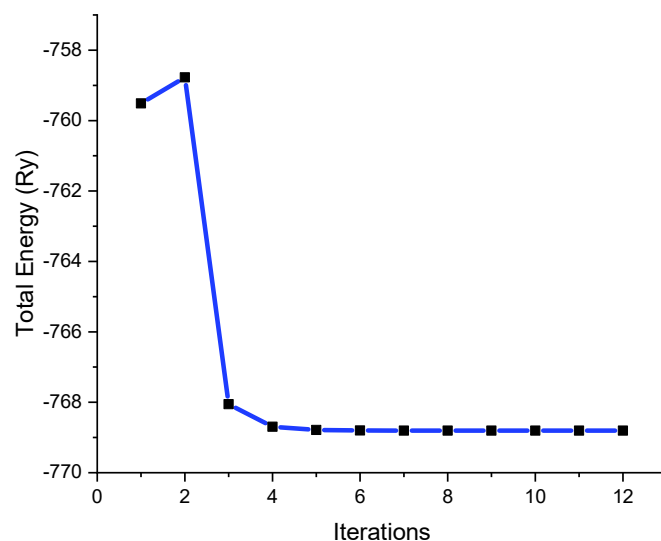


Fig 4.15: Convergence of total energy with respect to total energy of MNA.

### 4.3.2. Electronic property of MNA

The electronic structure calculation was performed using QE code with the following input parameters. The BZ sampling was done using the k-point grid of  $6 \times 4 \times 8$  according the Monkhorst -pack scheme. The convergence limit is chosen to be  $1 \times 10^{-6} \text{ Ry}$  with the PW kinetic energy cut-off of  $25 \text{ Ry}$  and charge density cutoff of  $225 \text{ Ry}$ . The calculations were performed using the relax structure of Urea in its ground state. The energy bands are calculated along the high symmetric k-path.

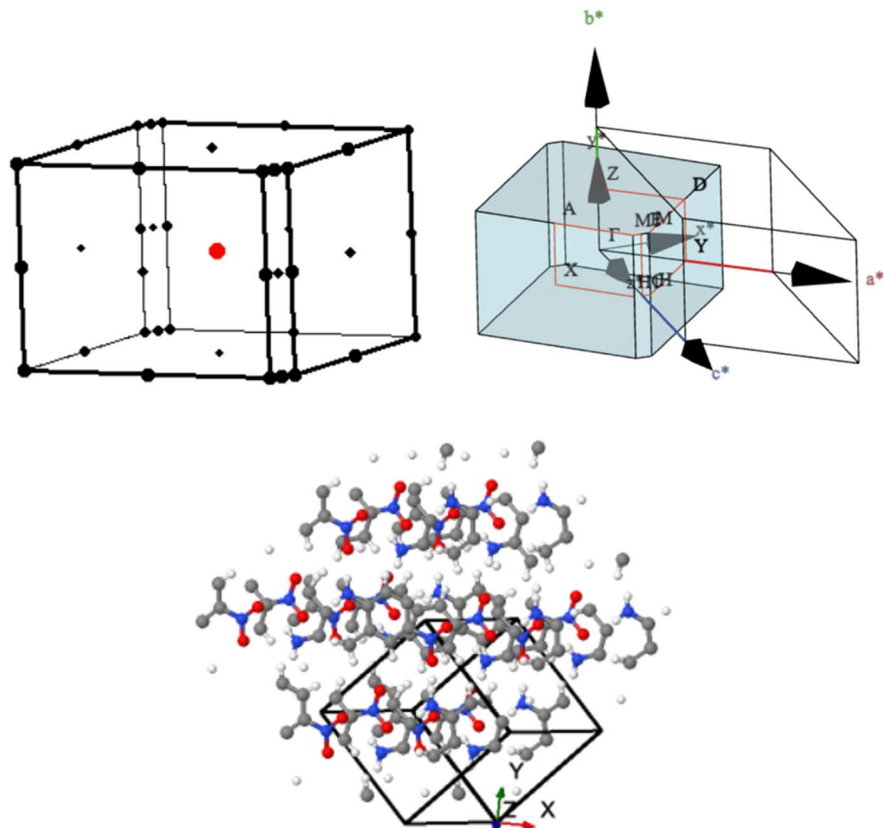


Fig 4.16: The high symmetric K-points and the unit cell of the bulk unit MNA in relaxed structure

The electronic band structure is plotted by keeping the fermi energy as the reference. The fermi energy calculated is  $2.1476 \text{ eV}$ . MNA in its crystal form has a direct band gap of  $\sim 2.2 \text{ eV}$  which agrees with the results available. The band structure reveals that MNA is an insulator. The periodicity of the band structure shows that MNA is a highly crystalline structure.

From the DOS plot it is seen that all the elements have relatively equal contribution to the total number of electrons.

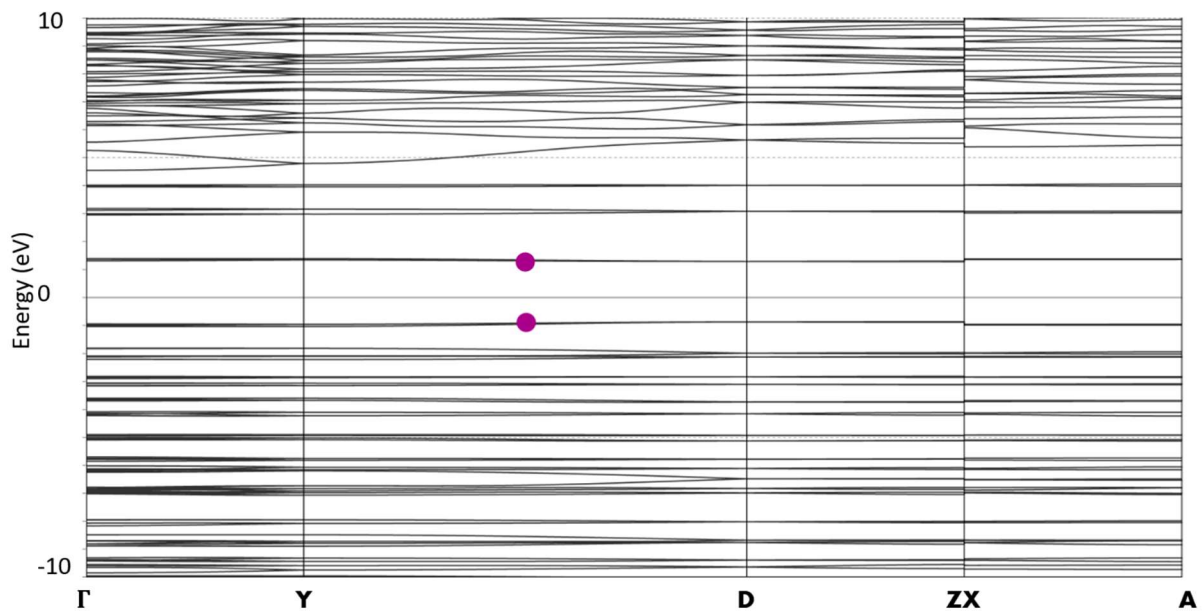


Fig 4.17: Band electronic band structure of MNA

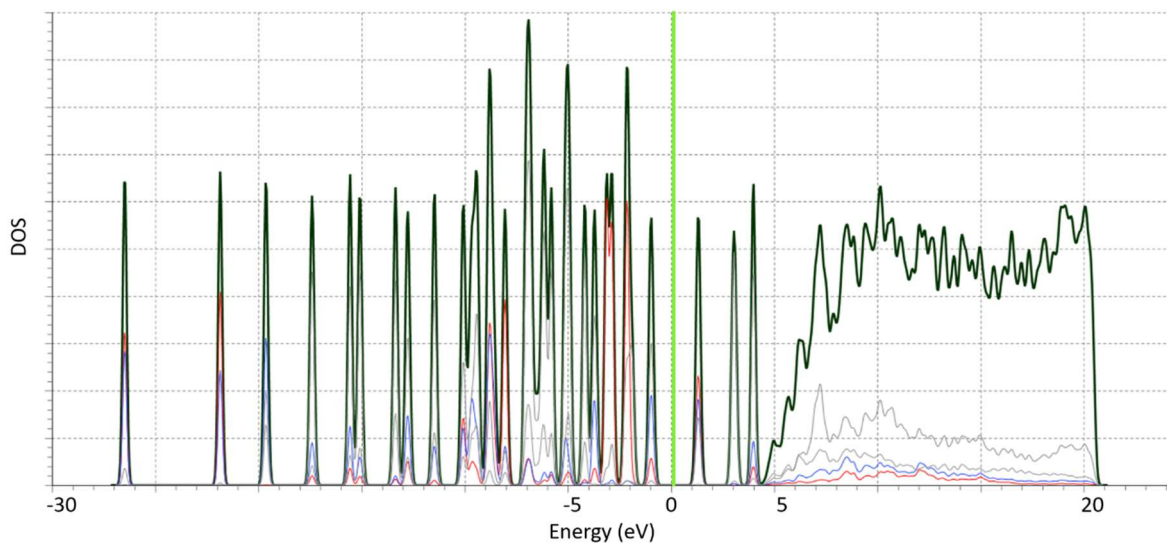


Fig 4.18: The Density of states (DOS) of MNA with fermi energy kept as reference.

From the PDOS it is found that the p orbital of nitrogen, carbon and oxygen has the maximum contribution in the bonding. The hydrogen bonding in MNA is less as compared to Urea. Thus, the PDOS gives a overall view of the bonding involved in the MNA molecule.

The total energy of the molecule in its ground state is  $-785.21 \text{ Ry}$  and the lowest occupied level is found to be  $4.2974 \text{ eV}$  and the highest occupied level is found to be  $1.6617 \text{ eV}$ .

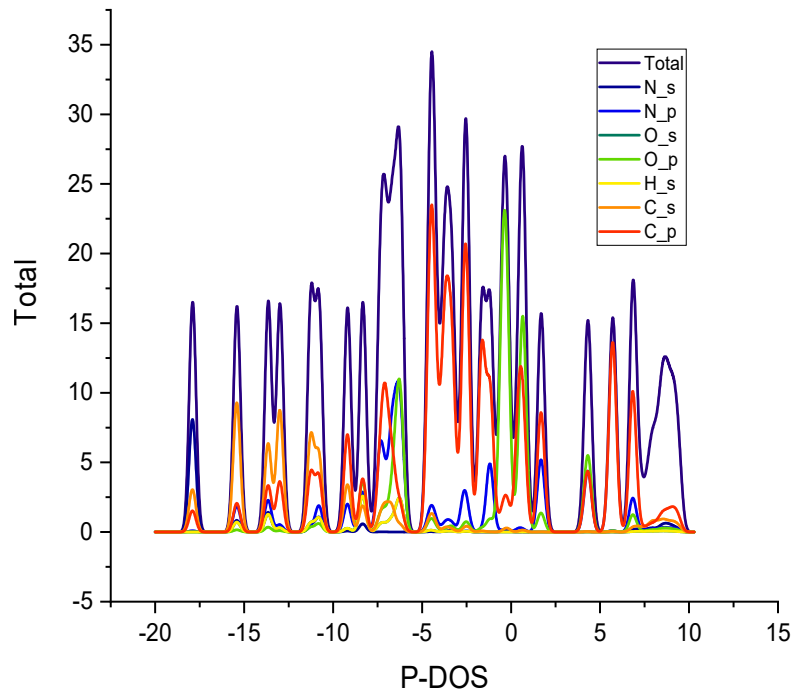


Fig 4.19: Projected density of states (PDOS) of MNA

#### 4.3.3. Absorption Spectra of MNA

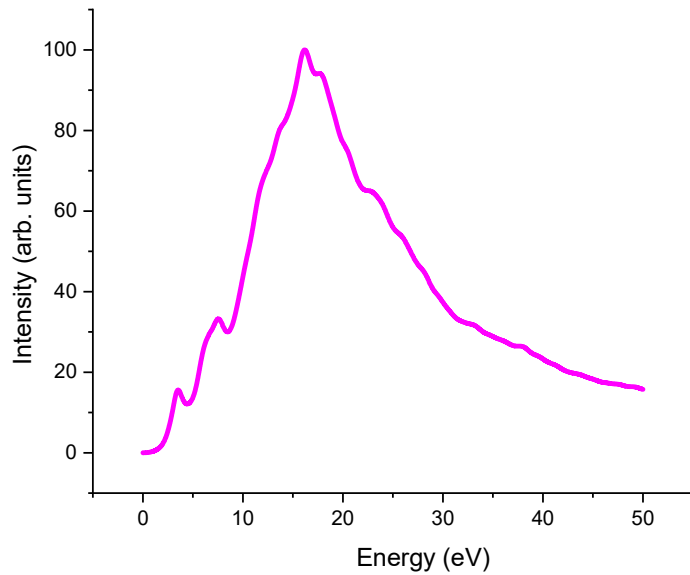


Fig 4.20: Absorption spectra of MNA molecule

The absorption spectra of MNA have been calculated by taking account of all the directions. The absorption spectrum of a molecule provides information about the wavelengths of electromagnetic radiation that are absorbed by the molecule as it transitions from a lower energy state to a higher energy state. Oscillator strength is a measure of the probability of a transition between two electronic states in a molecule. It quantifies the intensity of absorption bands in the absorption spectrum. Strong absorption bands with high

oscillator strength values correspond to transitions that are more probable and have higher transition dipole moments. The peaks at 3.6 eV (344.4005nm) and 7.5 eV (167.5462nm) correspond to a lower electronic transition. The peak at 16.17 eV (76.6754nm) corresponds to a higher electronic transition.

The results found agree with the experimental results and the results obtained in previous works [2] [36].

# CHAPTER 5

## First-principles calculations Tantalum Arsenide (TaAs)

### 5.1. Inorganic crystals

Inorganic crystals are crystalline structures which are composed of non-carbon-based compounds and exhibit a diverse array of properties and applications. From semiconductors to ceramics, inorganic crystals play pivotal roles in numerous fields, including electronics, optoelectronics, catalysis, and beyond. Inorganic crystals are relatively easy to work with the computational methods as compared to the organic crystals because of the following:

- **Symmetry:** Inorganic crystals tend to possess higher degrees of symmetry compared to organic crystals. Symmetry reduces the number of unique atoms and simplifies the crystal structure, making it easier to describe mathematically and computationally. Higher symmetry also allows for more efficient sampling of the Brillouin zone in reciprocal space.
- **Stronger Bonds:** Inorganic crystals typically involve stronger bonding interactions, such as ionic, covalent, or metallic bonds, compared to the weaker van der Waals interactions often found in organic crystals. These stronger bonds result in more well-defined structural motifs and energetically favourable configurations, simplifying the modelling of interatomic interactions.
- **Less Structural Complexity:** Inorganic crystals often exhibit simpler structural motifs and less structural complexity compared to organic crystals. This simplicity facilitates the use of idealized crystal structures, such as those described by high-symmetry crystallographic space groups, which require fewer parameters to describe.
- **Well-Defined Unit Cells:** Inorganic crystals typically have well-defined unit cells with clear lattice parameters and atomic positions. This regularity simplifies the setup of computational models and reduces the need for extensive structural optimization.
- **Less Sensitivity to Basis Set Size:** Inorganic crystals often require smaller basis sets to achieve converged results compared to organic crystals. This reduced sensitivity to basis set size simplifies the computational setup and reduces computational costs.

However, it is important to note that challenges may still arise, especially for complex or disordered inorganic systems, and careful consideration of computational parameters and methods is essential for obtaining accurate and reliable results.

## 5.2. Tantalum Arsenide (TaAs)

TaAs (Tantalum Arsenide) is an inorganic compound. It consists of tantalum (Ta) and arsenic (As) elements, which are both inorganic elements. TaAs crystallizes in a non-centrosymmetric structure, making it a topological material with interesting electronic and optical properties. TaAs belongs to the family of Weyl semimetals. It is notable as being the first topological Weyl semimetal that was identified and characterized by ARPES (Angle-resolved photoemission spectroscopy) [37] [38] [4].

## 5.3. Structural Parameters

TaAs crystallizes in the tetragonal I4<sub>1</sub>md space group. Ta<sup>3+</sup> is bonded to six equivalent As<sup>3-</sup> atoms. As<sup>3-</sup> is bonded to six equivalent Ta<sup>3+</sup> atoms to form a mixture of distorted edge, corner, and face-sharing TaAs<sub>6</sub> and AsTa<sub>6</sub> pentagonal pyramids [3] [39].

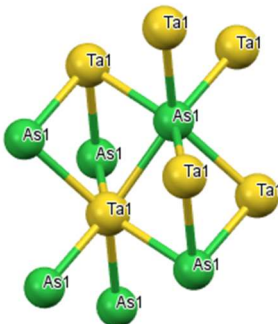


Fig 5.1: The Asymmetric unit cell of TaAs representing its bonding.

The bulk TaAs crystal is taken for calculation which consist of 8 atoms in a unit cell. This structure has 200 electrons which contribute to the electronic charge density of the molecule with 120 KS states.

The lattice parameters were fully optimized and the atomic positions are also relaxed and the lattice parameters are given as:

- $a = 3.44363\text{\AA}$  ;  $b = 3.44363\text{\AA}$  ;  $c = 11.73588\text{\AA}$
- $\alpha = \beta = \gamma = 90.0000^\circ$
- Unit-cell volume =  $139.170722\text{\AA}^3$

TaAs follows a primitive tetragonal crystal system having a point group  $42m$  and space group  $P4_2_1m$ .

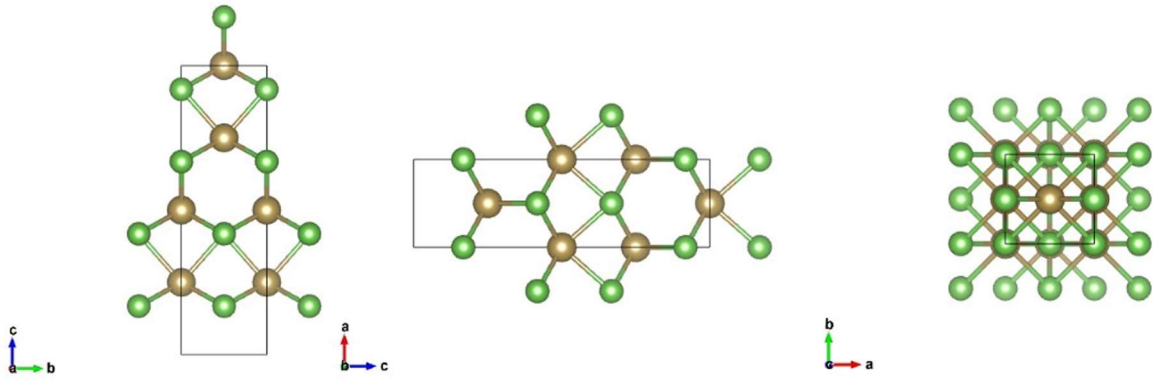


Fig 5.2: The TaAs crystal in different orientations

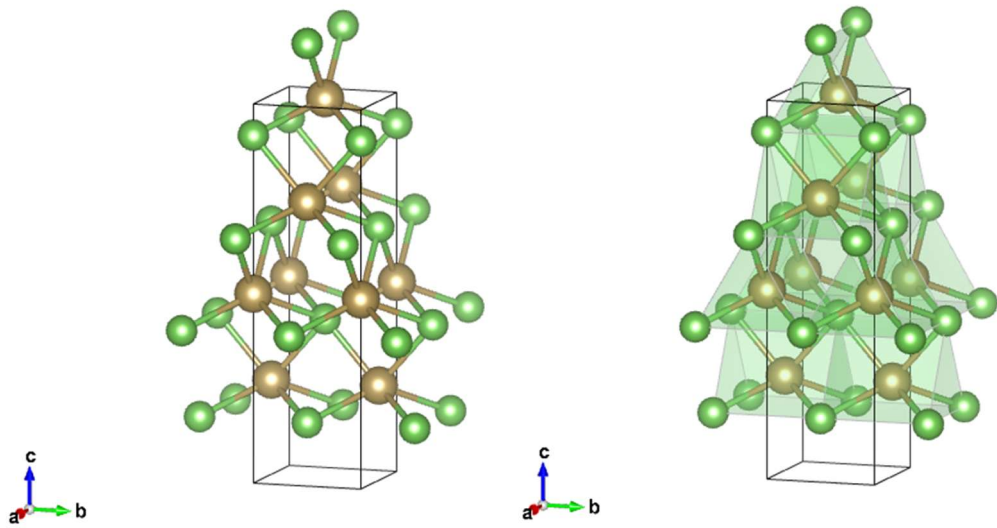


Fig 5.3: The TaAs crystal in bulk form

The simulated powdered diffraction pattern of TaAs exactly matches with the experimental XRD pattern which shows that the structure optimization is worked well in case of TaAs.

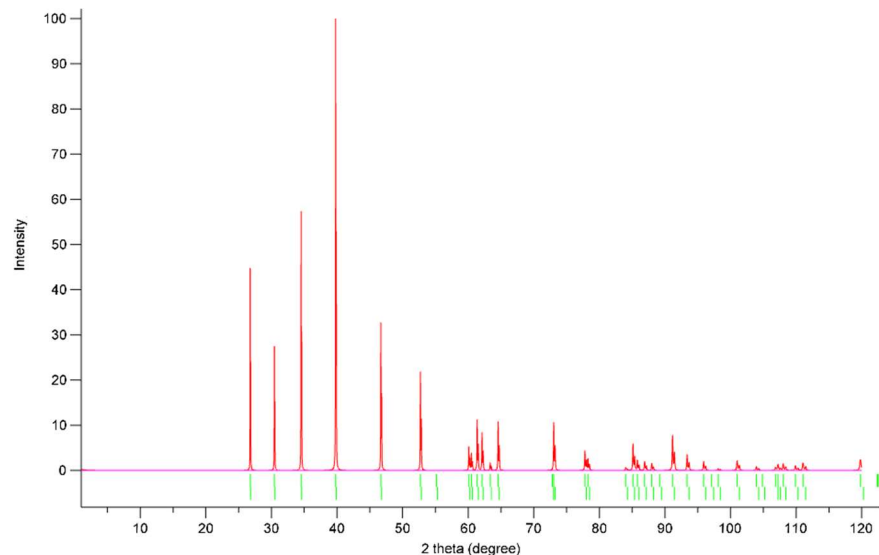


Fig 5.4: Simulated XRD of TaAs

The convergence for the Urea structure has been achieved in 9 iterations with total energy  $-650.32338369 \text{ Ry}$

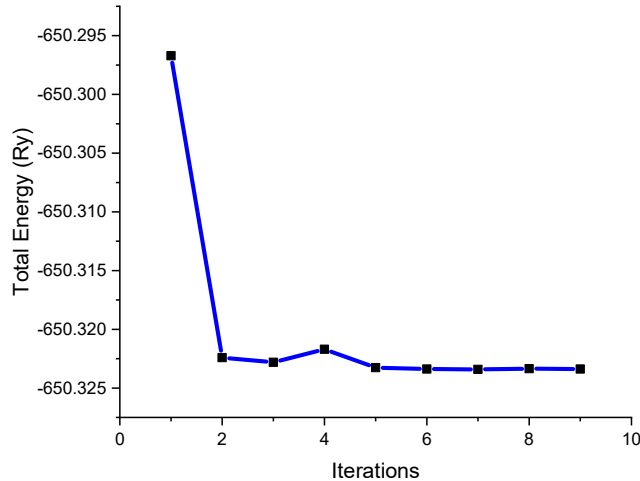


Fig 5.5: Convergence of total energy with respect to total energy of TaAs.

## 5.4. Mechanical Properties

The converged stress and pressure matrix is given as

- Total stress (Ry/ $\text{bohr}^3$ ) =  $\begin{matrix} -0.00821 & 0.000000 & 0.000000 \\ 0.000000 & -0.01100 & 0.000000 \\ 0.000000 & 0.000000 & 0.023672 \end{matrix}$

- Total pressure (Kbar) =  $\begin{matrix} -1208.26 & 0.000000 & 0.000000 \\ 0.000000 & -1619.48 & 0.000000 \\ 0.000000 & 0.000000 & 3482.37 \end{matrix}$
- Total pressure = 218.21 kbar
- Total density =  $61.80720 \frac{\text{g}}{\text{cm}^3}$
- Total Bulk Modulus = 175 Gpa.

From the above calculated parameter, one can say that TaAs have high hardness which is due to the presence of Ta and As atoms. It has a high strength due to the metallic bonding between Ta and As. Again, due to its metallic bonding it has a high bulk modulus and have reduced ductile property [40].

## 5.5. Electronic property of TaAs

The electronic structure calculation was performed using QE code with the following input parameters. The BZ sampling was done using the k-point grid of  $9 \times 9 \times 3$  according the Monkhorst -pack scheme. The convergence limit is chosen to be  $1 \times 10^{-6} \text{ Ry}$  with the

PW kinetic energy cut-off of 25 Ry and charge density cutoff of 225 Ry. The calculations were performed using the relax structure of TaAs in its ground state. The energy bands are calculated along the high symmetric k-path.

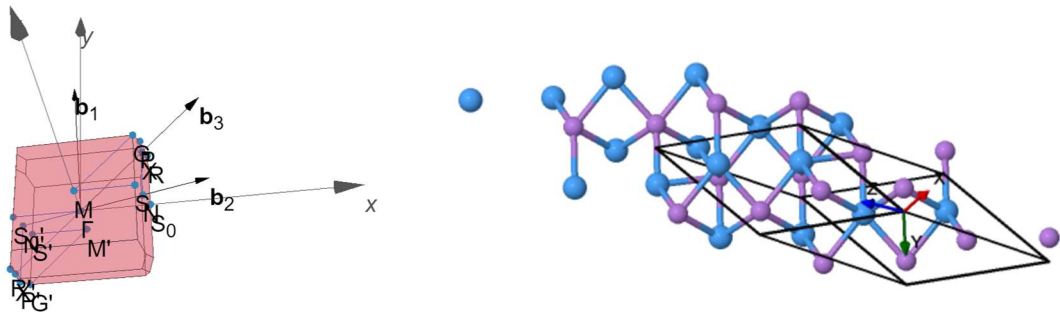


Fig 5.6: The high symmetric K-points and the unit cell of the bulk unit TaAs in relaxed structure

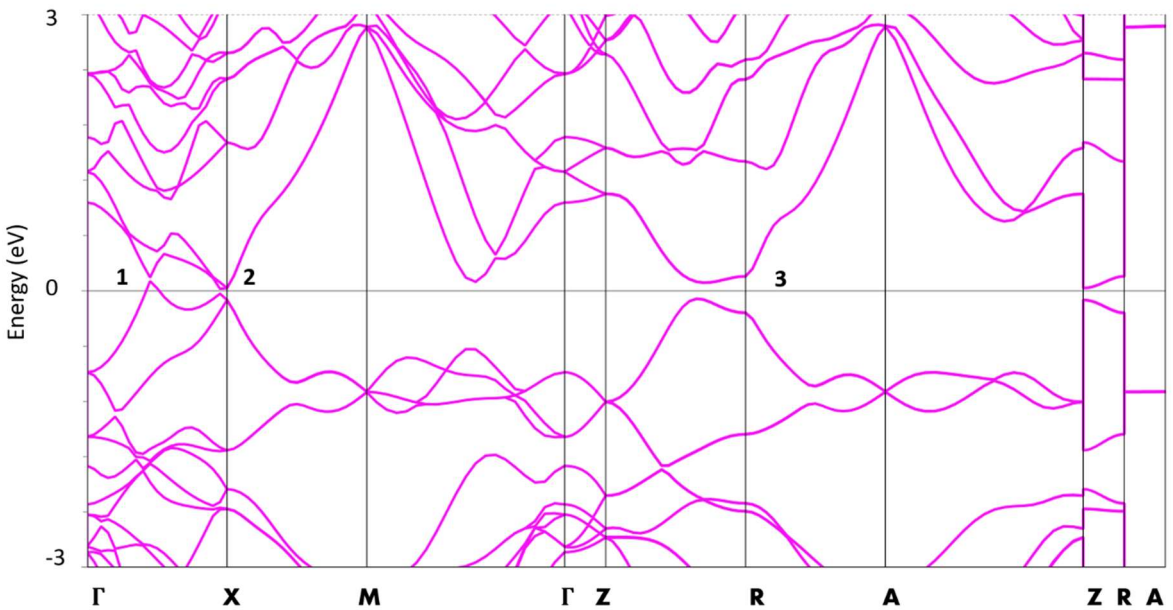


Fig 5.7: Band electronic band structure of TaAs

TaAs is known as a Dirac semimetal, a term used to describe materials whose band structure features Dirac nodes, which are points where conduction and valence bands meet linearly. In TaAs, these Dirac nodes occur at specific points in the Brillouin zone such as  $\Gamma$ X (point 1) and ZR (point 2) ban paths. One of the most remarkable features of TaAs is the existence of topological surface states. These surface states are a consequence of the non-trivial band topology of TaAs and are protected by certain symmetry properties (points 1,2 and 3). They typically form near the Fermi level and exhibit linear dispersion, like the Dirac cones found in graphene. The electronic band dispersion in TaAs typically shows few bands crossing the Fermi level, with distinct characteristics near the Dirac points. The behaviour of

these bands, such as their curvature and crossing points, provides insights into the material's electronic properties and its potential for applications in fields like spintronics and quantum computing. Experimental techniques such as angle-resolved photoemission spectroscopy (ARPES) and scanning tunnelling microscopy/spectroscopy (STM/STS) have been instrumental in probing the band structure of TaAs and confirming its topological nature and the calculated band structure is in agreement with the experimentally observed results. This calculated band structure has a band gap of 53.73 meV in point 2 ( $\Gamma$ X) and 0.18eV in point 3 (ZR) and this conforms that this is a Weyl semimetal. The electronic band structure and the DOS are plotted by keeping the fermi energy as reference. Fermi energy = 28.4993 eV. This calculated band structure without spin-orbit coupling has a slightly wider band gap as compared to the literature available, it might be due to the use for XC function in the particular calculation and the different codes as no literature is available for calculations done using QE for TaAs.

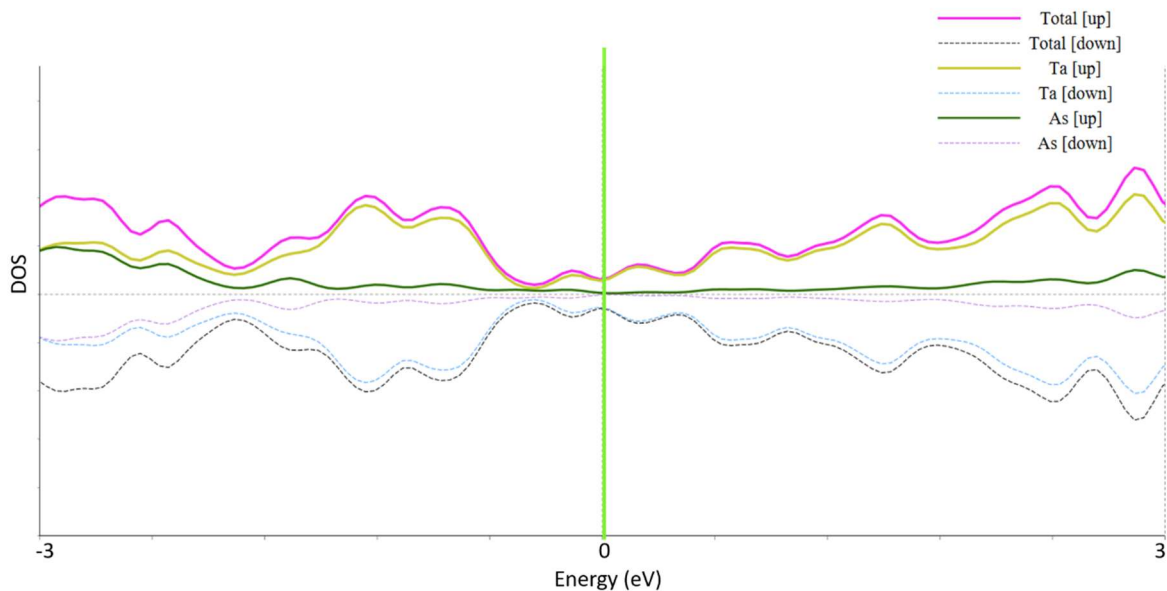


Fig 6: The Density of states (DOS) of TaAs with fermi energy kept as reference.

From the DOS plot it is clearly seen that the contribution of Ta is more in the density of states as compared to As.

The PDOS plot show that the d orbital of Ta and the d orbital of As involve in the maximum bonding. Other orbitals barely involves in bonding.

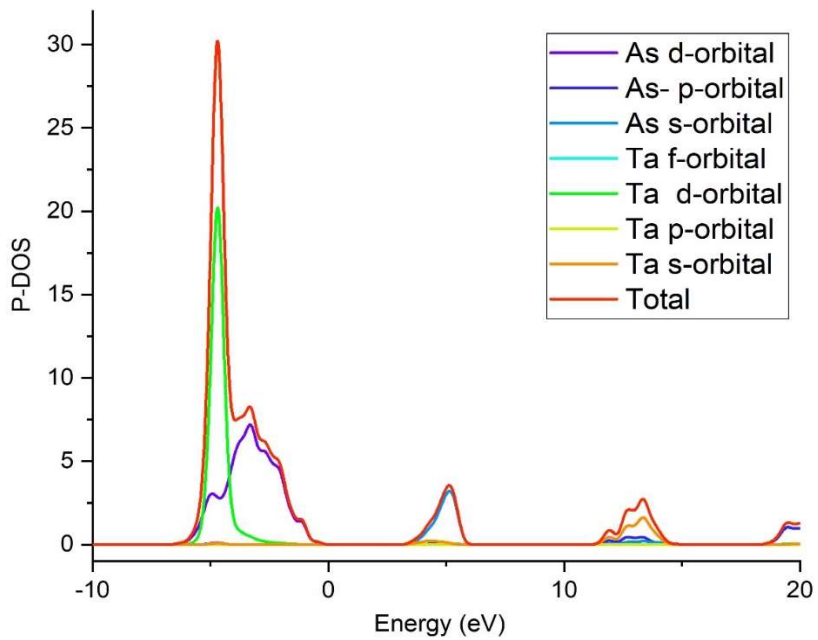


Fig 7: The Projected Density of states (PDOS) of TaAs

## 5.6. Magnetic properties

The total magnetization = 3.11 Bohr mag/cell. The variation of the total magnetization w.r.t the convergence is plotted.

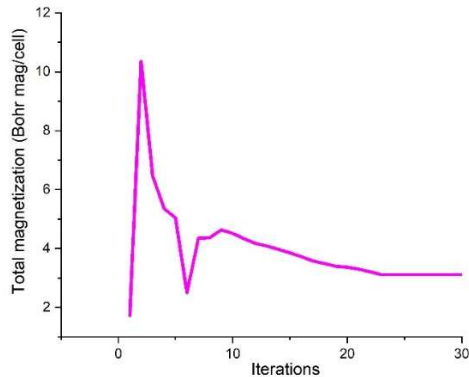


Fig 8: The variation of the total magnetization w.r.t the convergence

TaAs exhibit a large topological magneto-electric effect. This effect refers to the generation of an electric polarization in response to an applied magnetic field, and it arises due to the unique electronic band structure of TaAs. TaAs can also exhibit conventional magnetic ordering under certain conditions. For instance, TaAs can undergo a transition to a ferromagnetic state at low temperatures when doped with certain impurities or subjected to specific magnetic fields. TaAs has been found to display significant magneto-resistance, where the electrical resistance of the material changes in response to an applied magnetic field [4].

## 5.7. Thermodynamic property

From the experimental results this ground state of the molecule is stable in normal condition even though it has a endothermic energy exchange in a reaction. The ground state energy and the internal of TaAs is given below along with the enthalpy.

- The total energy of the system : -4513.88434915 Ry
- The total internal energy of the system : -4513.87450529 Ry
- The average enthalpy of the system : -4964.3315049892 Ry

The structure of the TaAs crystal is observed in various phases and in different binary combination but that form the DFT calculation this structure is the most stable and more crystalline phase.

## 5.8. Absorption spectra

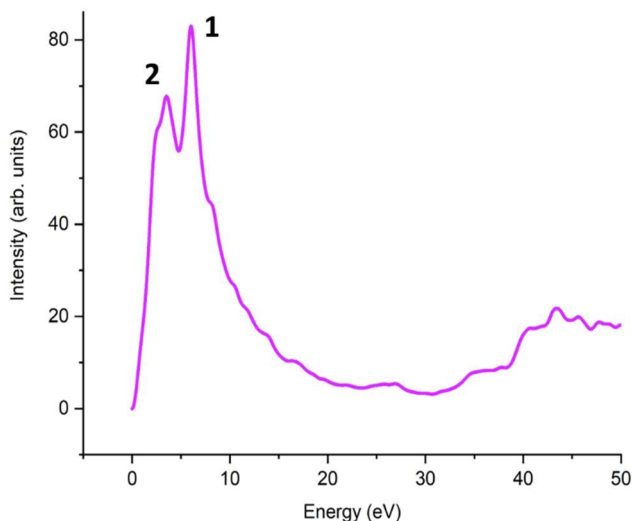


Fig 9: Absorption spectra of TaAs molecule

The absorption spectra of TaAs have been calculated by taking account of all the directions. From the absorption spectra it is seen that there are two distinct peaks at 6 eV (1) (206.6403 nm) and 3.6eV (2) (344.4005 nm), which shows that there is an electronic transition between those two states. This sharp peak in those regions specifies the high probability of electronic transition in that region. This presence of well-defined absorption peaks at certain wavelengths indicates that the material has electronic states that can efficiently interact with incident light to generate nonlinear optical effects. So TaAs has potential NLO application as mentioned in literature.

The results found agree with the experimental results and the results obtained in previous works [37] [4] [41] [42].

# CHAPTER 6

## Conclusion and further work

### 6.1. Conclusion

To conclude, this work presents the theoretical studies of NLO materials based on DFT using PW basis set.

The crystal structure of urea has been relaxed and optimized using vc-relax method and the convergence of total energy is achieved in 8 iterations with the ground state ground energy  $\sim 713.21 \text{ Ry}$ . The band structure of Urea is calculated using the  $3 \times 3 \times 9$  k-point grid and the band gap is found to be  $\sim 5.4 \text{ eV}$  and the Fermi energy is found to be  $1.502 \text{ eV}$ . From the DOS and PDOS plots it is found that the p- orbital of nitrogen and oxygen has maximum contribute to electrons in the conduction and valance band.

The crystal structure of MNA has been relaxed and optimized using vc-relax method and the convergence of total energy is achieved in 12 iterations with the ground state ground energy  $768.80528942 \text{ Ry}$ . The band structure of MNA is calculated using the  $6 \times 4 \times 8$  k-point grid and the band gap is found to be  $\sim 2.2 \text{ eV}$  and the Fermi energy is found to be  $2.1476 \text{ eV}$ . From the DOS plot it is found that the all the elements have similar contribution in the contribute to electrons in the conduction and valance band. From the PDOS plot it is found the p orbital of nitrogen, carbon and oxygen has maximum contribution in the bonding. The absorption spectra is calculated using the coupled linear-response TDDFPT equations. From that it is found that the peaks at  $3.6 \text{ eV}$  ( $344.4005 \text{ nm}$ ) and  $7.5 \text{ eV}$  ( $167.5462 \text{ nm}$ ) correspond to a lower electronic transition. The peak at  $16.17 \text{ eV}$  ( $76.6754 \text{ nm}$ ) corresponds to a higher electronic transition.

The crystal structure of TaAs has been relaxed and optimized using vc-relaxed method and the convergence of total energy is achieved in 9 iterations with the ground state ground energy  $650.32338369 \text{ Ry}$ . The band structure of TaAs is calculated using the  $9 \times 9 \times 3$  k- point grid and found that the point  $1(\Gamma X)$  and  $2(ZR)$  have a direct band gap of  $53.73 \text{ meV}$  and  $0.18 \text{ eV}$  which confirms that it is a Wely semimetal and the Fermi energy is found to be  $28.4993 \text{ eV}$ . From the DOS plot it is clearly seen that the contribution of Ta is more in the DOS as compared to As and the PDOS plot show that the d orbital of Ta and the d orbital of As involve in the maximum bonding. The total stress matrix and pressure matrix has been calculated and found TaAs has a high degree of hardness. The total magnetization is found to be  $3.11 \text{ Bohr magneton/cell}$  which shows the TaAs exhibits a large topological magneto-electro character. The enthalpy of the system is found to be  $\sim 4964.3315049892 \text{ Ry}$ . The absorption spectra is calculated using the coupled linear-response TDDFPT equations from

that it is found that there are two distinct peaks at  $6\text{ eV}$  (1) ( $206.6403\text{ nm}$ ) and  $3.6\text{ eV}$  (2) ( $344.4005\text{ nm}$ ), which shows that there is an electronic transition between those two states. This sharp peak in those regions specifies the high probability of electronic transition in that region.

## 6.2. Further work

The materials chosen i.e. Urea, MNA and TaAs have potential applications in non-linear optics. The calculation that are done in this work is the preliminary calculation to find other properties like linear optical response, dielectric function, Nonlinear Susceptibility, Nonlinear Coefficient, hyperpolarizability and other properties using more advanced codes like Elk code, VASP, Materials studio etc. Apart from this TaAs has a huge scope of study in other applications like spintronics, photonics, optoelectronics, topological insulators, and energy storage and conversion. Using the data and results from this work further calculations can be carried out to find the applied properties.

## References

- [1] M. D. A.r. omidi, "optical properties of phenanthrene: a dft study for comparison between linear and nonlinear regimes," *solid state communications*, vol. 234–235, pp. 1-9, may 2016.
- [2] P. A. G. P. Hermet, "first-principles study of the dynamical and nonlinear optical properties of urea single crystals," *phys. Chem. Chem. Phys.*, pp. Vol 12, issue 4, 835-843, 2010.
- [3] H. B. A. E. Parthe, "the transposition structure of nb as and of similar monophosphides and arsenides of niobium and tantalum.," *acta crystallographica* , p. 1095–1101, 1963.
- [4] Z. K. L. Y. S. H. P. H. F. Y. T. Z. B. Z. Y. Z. Y. F. G. M. R. D. P. Z. H. S.-k. M. C. F. B. Y. & Y. L. C. L. X. Yang, "weyl semimetal phase in the non-centrosymmetric compound taas," *nature physics*, pp. 728-732, august 2015.
- [5] A. J. K. Susi lehtola, "free and open source software for computational chemistry education," *wires computational molecular science*, 2022.
- [6] T. Kaewmaraya, "first-principles studies of materials," isbn 978-91-554-9247-2, uppsala, sweden., 2015.
- [7] P. M. Chaikin and t. C. Lubensky, principles of condensed matter physics (4th print ed.), cambridge: cambridge university press, 2007.
- [8] P. G. C. P. N. Marzari, "atomistic computer modeling of materials (sma 5107)," mit open learning, spring 2005 .
- [9] C. D. Sherrill, "introduction to hartree-fock molecular orbital theory," georgia tech, center for computational molecular science and thechenology.
- [10] J. G. Lee, computational materials science -an introduction second edition, taylor & francis, 2017.
- [11] W. Kohn, density functional theory." introductory quantum mechanics with matlab: for atoms, molecules, clusters, and nanocrystals, 2019.
- [12] D. M. C. A. B. J. Alder, "ground state of the electron gas by a stochastic method," *physical review letters*, vol. 45, p. 566, aug 1980.
- [13] W. K. A. L. J. Sham, "self-consistent equations including exchange and correlation effects," *physical review journals archive*, vol. A1133, p. 140, nov, 1965.
- [14] J. P. P. A. Y. Wang, "accurate and simple analytic representation of the electron-gas correlation energy," *physical review b*, vol. 45, 2018.
- [15] G. K. A. J. Furthmüller, "efficient iterative schemes for ab initio total-energy calculations using a plane-wave basis set," *physical review b*, vol. 54, p. 11169, 1996.
- [16] K. Refson, "introduction to dft and the plane-wave pseudopotential method," epcc, part of the university of edinburgh, university college london, 23 apr 2014.

- [17] N. A. B. 6. Castep developers group, "plane waves, unit cell, k-points and all that," castep with support with esu, durham, 2021.
- [18] H. J. M. A. J. D. Pack, "special points for brillouin-zone integrations," *physical review b*, vol. 13, p. 5188, 1976.
- [19] C. G.-n. Tutorial, "an introduction to pseudopotentials," university of cambridge, 23 sep 2009.
- [20] A. D. Corso, "modern pseudopotentials: an introduction," sissa and democritos, trieste (italy).
- [21] W. Quester, artist, *comparison of a wavefunction in the coulomb potential of the nucleus (blue) to the one in the pseudopotential (red). The real and the pseudo wavefunction and potentials match above a certain cutoff radius .. [art]*. Wikipedia, 2024, january 15.
- [22] W. Klopper, "scf methods, basis sets, and integrals lecture i: self-consistent field methods," abteilung für theoretische chemie, institut für physikalische chemie karlsruher institut für technologie (kit), 2022.
- [23] P. B. S. B. N. C. M. C. R. C. C. C. D. C. G. C. M. D. I. A. D. C. A. E. A. Giannozzi, "quantum espresso: a modular and open-source software project for quantum simulations of materials.," *journal of physics: condensed matter*, vol. 39, no. 21, p. 395502, 2009.
- [24] S. Narasimhan, "the "self consistent field" scf) loop and some relevant input parameters for quantum--espresso," ictp, 2011.
- [25] P. B. S. B. N. C. M. C. R. C. C. C. D. C. G. C. M. D. I. A. D. C. A. Giannozzi, "quantum-espresso.org," quantum-espresso, [online]. Available: [https://www.quantum-espresso.org/doc/input\\_pw.html](https://www.quantum-espresso.org/doc/input_pw.html).
- [26] Pranabdas, "pranabdas.github.io," [Online]. Available: <https://pranabdas.github.io/espresso/category/hands-on/>.
- [27] I. Timrov, "time-dependent density functional perturbation theory: calculation of absorption spectra of molecules," theory and simulation of materials (theos), and national centre for computational design and discovery of novel materials (marvel), école polytechnique fédérale de lausanne (epfl), lausanne, switzerland, 2017.
- [28] R. G. D. R. A. S. B. Osman baris, malcioglu, "turbotddft – a code for the simulation of molecular spectra using the liouville-lanczos approach to time-dependent density-functional perturbation theory," *computer physics communications*, 2011.
- [29] J. J. Paul, "computational-condensed-matter-physics," 2023. [online]. Available: [https://github.com/johnpaulj1509/computational-condensed-matter-physics/tree/main/quantum\\_espresso](https://github.com/johnpaulj1509/computational-condensed-matter-physics/tree/main/quantum_espresso).
- [30] F. I. Koichi momma, "vesta: a three-dimensional visualization system for electronic and structural analysis," *journal of applied crystallography*, vol. 41, no. 3, pp. 653-658, 2008.

- [31] A. Kokalj, "xcrysden—a new program for displaying crystalline structures and electron densities," *journal of molecular graphics and modelling*, vol. 17, pp. 176-179, 2000 (online).
- [32] D. J. F. Van rossum g, "python reference manual," *centrum voor wiskunde en informatica amsterdam.*, 1995.
- [33] S. Nishihara, *burai 1.3 is a gui system for quantum espresso*, <https://nisihara.wixsite.com/burai>, 2016.
- [34] O. Corporation., *origin(pro)*, 2018.
- [35] K. D. A. C. Z.-w. B. Civalleri, *ab initio investigation of structure and cohesive energy of crystalline urea*. *Journal of physical chemistry,*, 2007.
- [36] M. D. A. A. R. Omidi, "a dft study of linear and nonlinear optical properties of 2-methyl-4-nitroaniline and 2-amino-4-nitroaniline crystals," *the journal of physical chemistry c*, vol. 119, no. 28, pp. 16263-16275, 2015.
- [37] M. E. Dadsetani, " optical distinctions between weyl semimetal taas and dirac semimetal na3bi: an ab initio investigation," *j. Electron. Mater*, vol. 45, p. 867–5876, 2016.
- [38] H. W. B. F. X. W. H. M. J. M. P. R. X. H. L. Z. G. C. Z. F. X. D. T. Q. A. H. D. B. q. Lv, "experimental discovery of weyl semimetal taas," *physical review x*, vol. 5, no. 3, 2015.
- [39] T. M. Project, *as-ta*, the materials project.
- [40] S. P. O. G. H. W. C. W. D. R. S. D. S. C. D. G. D. S. G. C. A. K. A. P. Anubhav jain, "commentary: the materials project: a materials genome approach to accelerating materials innovation," *apl materials* , 2013.
- [41] L. Z. Y. L. P. W. D. C. Z. Y. H. L. M. X. H. W. Z. F. X. D. A. G. C. Xiaochun huang, "observation of the chiral-anomaly-induced negative magnetoresistance in 3d weyl semimetal taas," *physical review x*, vol. 5, 2015.
- [42] J. N. N. E. Al, "thin film taas: developing a platform for weyl semimetal devices," *matter*, vol. 6, no. 9, pp. 2886-2899, 2023.
- [43] L. Z. L. W. D. C. Y. H. L. Xiaochun huang, "observation of the chiral-anomaly-induced negative magnetoresistance".